MECHANICAL CHARACTERIZATION AND MODELING OF THREE-DIMENSIONAL CARBON NANOTUBE STRUCTURES

by

Wenjie Zhao

A dissertation submitted to the Faculty of the University of Delaware in partial fulfillment of the requirements for the degree of Doctor of Philosophy in Mechanical Engineering

Summer 2015

MECHANICAL CHARACTERIZATION AND MODELING OF THREE-DIMENSIONAL CARBON NANOTUBE STRUCTURES

by

Wenjie Zhao

Approved:

_____

Suresh G. Advani, Ph.D.
Chair of the Department of Mechanical Engineering

Approved:

_____

Babatunde A. Ogunnaike, Ph.D.
Dean of the College of Engineering

Approved:

_____

James G. Richards, Ph.D.
Vice Provost for Graduate and Professional Education

I certify that I have read this dissertation and that in my opinion it meets the academic and professional standard required by the University as a dissertation for the degree of Doctor of Philosophy.

Signed:

_____

Jonghwan Suhr, Ph.D.
Professor in charge of dissertation

I certify that I have read this dissertation and that in my opinion it meets the academic and professional standard required by the University as a dissertation for the degree of Doctor of Philosophy.

Signed:

_____

X. Lucas Lu, Ph.D.
Member of dissertation committee

I certify that I have read this dissertation and that in my opinion it meets the academic and professional standard required by the University as a dissertation for the degree of Doctor of Philosophy.

Signed:

_____

Bingqing Wei, Ph.D.
Member of dissertation committee

I certify that I have read this dissertation and that in my opinion it meets the academic and professional standard required by the University as a dissertation for the degree of Doctor of Philosophy.

Signed:

_____

Daniel O'Brien, Ph.D.
Member of dissertation committee

ACKNOWLEDGMENTS

I would like to thank my advisor, Dr. Jonghwan Suhr, and Dr. X. Lucas Lu for the exceptional resources and professional guidance they have provided me with over the years. It has truly been the honor to work together with Dr. Suhr and Dr. Lu and to share their scientific vision, perspective, wisdom, and insights. I would also like to thank Dr. Bingqing Wei for his guidance and support for my Ph.D career. I am also very grateful to Dr. Daniel O'brien who is my committee member throughout last three years. He has provided me with intellectual scientific input with great patience.

I express sincere appreciation to Dr. Pulickel Ajayan. As the principle investigator of MURI grant (U.S. Air Force Office of Scientific Research, FA9550-12-1-0035), he has spent extensive time devoting himself to the project. It has been a great privilege for me to work on the MURI project throughout the last four years. I would also like to take the opportunity to thank Dr. Mauricio Terrones, Dr. Ana L. Elias and Lakshmy P. Rajukumar for providing me the cutting-edge materials.

I am indebted to my mother, grandparents and uncle, Qingping, for their endless support and encouragement over these past years. I am forever grateful to their constant love. I would also like to thank my boyfriend, Zhiyu Cai for his enlightening suggestion for my career planning.

TABLE OF CONTENTS

LIST OF TABLES

LIST OF FIGURES

ABSTRACT

The exceptionally mechanical properties reported for carbon nanotubes (CNTs) has stimulated the research in the development of three-dimensional (3D) CNT based architectures (i.e. sponges, foams and aerogels). The production of engineered 3D CNT structures, with controlled architecture, are predicted to be one of the most desirable steps for building next-generation carbon-based functional materials. Before these predicted extraordinary properties at the nanoscale are realized in macroscale, considerable characterization and modeling research is necessary. This research work seeks to obtain a fundamental understanding of the mechanical properties and ultrastructure-property relations in 3D CNT materials and their composite through integrated mechanical characterization as well as development of constitutive model for the elastic properties of 3D CNTs. Ultimately, the characterization results and the establishment of structure-property relationships will guide the future design of 3D CNT materials.

In this work, systematical mechanical characterization, especially for the viscoelastic properties, was performed on the three types of 3D multiwalled CNTs (MWNT) sponge. The as-fabricated materials includes 3D boron doped MWNT (CBxMWNT), nitrogen doped MWNT (N-MWNT) and undoped-MWNT sponge. The doping strategy during the fabrication of CBxMWNT and N-MWNT generates the covalent junctions between CNTs and differentiate their ultrastructure from that of undoped-MWNT. Based on mechanical and microscopic characterization results, a microstructure informed continuum constitutive modeling was developed to describe

the hyperelastic behavior of 3D CNTs with covalent junctions and their structure-property relationships. To further reveal the application of 3D CNT sponge, 3D CNT reinforced polydimethylsiloxane composites were synthesized and fabricated. The effective reinforcement modulus of 3D CNT inside the composite was estimated.

Chapter 1

INTRODUCTION

1.1 Motivation and Scope

Nanomaterials such as carbon nanotubes (CNTs) have become the face of new and emerging technologies [1–4]. Numerous studies have shown that these outstanding mechanical properties would make CNTs assemblies competitive materials or ideal filler materials for composites in various engineering applications. However, presently realized mechanical properties of CNT macrostructures is far below that of individual CNTs due to the weak interaction between CNTs for structure integrity [5,6]. As a result of that, most CNT production today is used in bulk composite material and thin films, which rely on unorganized CNT architectures having limited properties, such as dispersed CNT powders [4]. Therefore, the issue of translating the exceptional properties of individual CNT to key applications remains a challenge nowadays.

To conquer these difficulties, researchers proposed to create controllable three-dimensional (3D) CNT architectures that are predicted to expand the CNT's superior properties to the third dimension [7,8]. Theoretically, compared to 2D CNT assemblies, the 3D architectures would experience a significant enhancement in chemical, electrical and mechanical properties due to increased active material per projected area and inter-tube interaction or covalent bonding in all dimensions [7,8]. A few 3D CNT structures of random entangled CNTs have been successfully fabricated [9–11]. The randomly networked CNTs form a 3D scaffold-like structure and the

highly porous spongy-like solids exhibit excellent dimensional stability in compression and introduce better energy absorbing capability into the composite system as a filler [7]. Covalently bonded 3D hierarchical CNT sponges have been successfully fabricated as well, in which CNTs can function as “building blocks” and being “welded” together with molecular junctions [12–15]. It is predicted that if the interconnections between CNTs could be controllable by scalable methods, the new types of 3D CNT solids could be created with novel properties. However, to date, engineering such 3D structures in scalable synthetic processes still remains a challenge and their mechanical properties including the influence of the covalent bonding has not been fully understood [13].

As scientists and engineers seek to make practical materials and devices from new developed 3D nanostructure, understanding material behavior across length scales from the microscopic to macroscopic levels is required. Knowledge of how the covalent bond or junctions influences the CNT assemblies properties as well as mechanical properties of composites reinforced with 3D CNTs of different topologies are needed to realize the potential for application of 3D CNTs and their composites. Compared with conventional CNT assemblies, the creation of 3D CNTs gives rise to the change in the morphologies from microscale to macroscale and poses new challenges in the characterization and modeling work. Unlike traditional one or two dimensional (1D or 2D) CNTs, the mechanical properties, such as modulus, strength and buckling were usually characterized by direct measurement [16–18], obvious difficulties are encountered in testing the 3D covalent bonded CNTs, of which the initial straight tubular morphologies are permanently changed. In addition, the properties of CNT and its assemblies in general, are highly ultrastructure dependent

although it still remains technical challenging to identify the roles of each individual factors through experiments. With the introduction of covalent junctions, property-ultrastructure relationships of CNT network become more elusive. This research work seeks to obtain a fundamental understanding of the mechanical properties and morphology-property relations in 3D CNT materials and their composite through integrated mechanical characterization as well as development of constitutive model for the elastic properties of 3D CNTs. Ultimately, the characterization results and the establishment of structure-property relationships will guide the future design of 3D CNT materials.

Chapter 1 provides a concise review of recent advances in CNTs, especial 3D CNTs, and their composites, examining the research work reported in the literature on structure as well as characterization results for CNTs and their composites. Chapter 2 reports our characterization work on the 3D CNT sponges' mechanical behavior under compression, with special emphasis on the viscoelastic properties. Chapter 3 develops a microstructure informed continuum constitutive model to interpret the hyperelastic behavior of 3D CNT sponge with covalent junctions and predict the structure-property relations. Chapter 4 systematically investigates the viscoelastic behavior of 3D CNT reinforced composites and estimates the effective reinforcement of 3D CNT embedded in the composites.

1.2 Advanced in 3D Carbon Nanotubes and Their Composite

Since their discovery in 1991 [19], CNTs have been the subject of numerous research works due to their unique properties, such as high electrical conductivities, excellent thermal conductivities, and outstanding mechanical properties compared to

most traditional materials [1,20]. The mechanical properties of individual CNTs as well as polymer composites with addition of CNTs as fillers have been characterized in both compression [18,21] and tension [22,23]. For individual CNT, the elastic modulus approaching 1TPa and a tensile strength of 100 GPa has been measured [23]. It also exhibits remarkable reversibility under large sustaining deformations and deformation without damage [18,24,25]. It has been reported that multiwalled CNT (MWNT) polymer composites reach conductivities as high as 10000 S m^{-1} at 10 wt% loading due to their high aspect ratio to form a percolation network [26] . For load-bearing applications, adding ~1 wt % MWNT to epoxy resin can enhance both stiffness and fracture toughness without compromising other mechanical properties [4]. Organized 2D CNT architectures such as vertically aligned forests, sheets and yarns are also expected to scale up the properties of individual CNTs and realize new functionalities [27–29].

Widespread CNT researches also predicted that CNTs would have lots of potential applications, such as energy storage media as fuel cells, battery [3], novel biosensors in health care [30] and environmental-friendly materials [31]. The CNTs are also widely utilized as the strongest or stiffest elements in nanoscale devices [24]. Additionally, the production capacity of CNTs that exceeds several thousand tons per year presently shows the worldwide commercial interest in this nanoscale material [4].

With the growing demand of CNT products and development of nanotechnology, over the past decades, engineered 3D CNT are one of the most compelling subjects under study. It is predicted that the production of engineered 3D CNT structures, with controlled architecture, is one of the most desirable steps for building next-generation carbon-based functional materials [14]. The existing 3D CNT

based architectures are mostly in the form of sponges, foams and aerogels [7,10,12–14,32–35]. The features of lightweight, porous the 3D CNT materials would enable their utilities in environmental-friendly applications [13,14,36]. The enhanced energy dissipation ability can be utilized in the microelectromechanical devices and energy absorption membranes [37]. The large surface area of 3D CNTs, especially with covalent interconnections was predicted to generate extraordinary electrical and mechanical properties in all the dimensions [8]. The exceptional physical properties of carbon nanotubes also present the opportunity to develop multifunctional CNT composites with tailored physical and mechanical properties. It has been reveal that the 3D CNT sponge may provide a way for fabrication of highly conductive composite with minimum CNT addition [35]. Overall, the systematic researches into the advances of 3D CNTs and their composites are still limited and in its initial stage, further studies are necessary to reveal their unique and extraordinary characteristics.

1.3 Atomic Structure and Morphology of Carbon Nanotube

1.3.1 Carbon Nanotube Structure

The atomic structure of CNTs is described in terms of the tube chirality, or helicity, which is defined by the chiral vector, $\overline{C_h}$, and the chiral angle, θ. In Figure 1.1a, we can visualize cutting the graphite sheet along the dotted lines and rolling the tube so that the tip of the chiral vector touches its tail. The chiral angle determines the amount of "twist" in the tube [20]. The chiral vector, often known as the roll-up vector, can be described by the following equation:

$$\overline{C_h} = n\overline{a_1} + n\overline{a_2}$$

where the integers (n, m) are the number of steps along the ziz-zag carbon bonds of the hexagonal lattice and $\overline{a_1}$, $\overline{a_2}$, are unit vectors, shown in Figure 1.1a ,

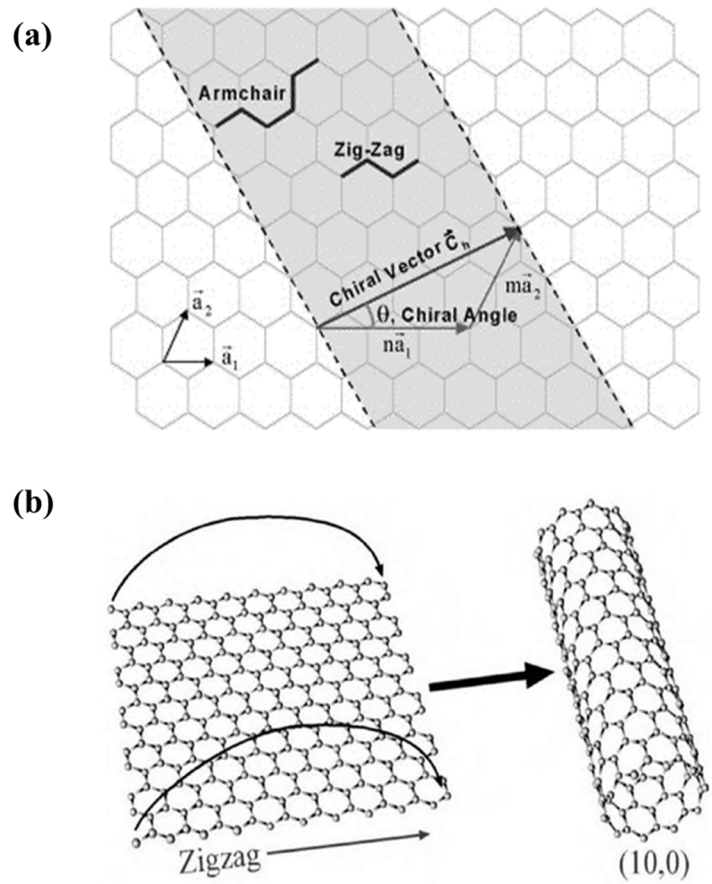

Figure 1.1 Schematic diagrams showing how a hexagonal sheet of graphite is "rolled" to form a CNT [20,38].

CNTs can be visualized as a sheet of graphite that has been rolled into a tube. CNTs exist as either single-walled or multi-walled structures. Each SWCNT is uniquely labeled with a pair of integers (n, m) describing its chirality (Figure 1.1b). The diameter of the SWCNT has the range of several nanometer and length up to

millimeters. A multi-walled CNT (MWNT) consists of concentric layers of cylinders around a common central hollow axil and the graphite layers have a 0.34nm interlayer distance. The outer diameter of MWCNTs ranges from 5nm to 30nm or more with several concentric layers [39].

To alter and extend the CNT's mechanical and electronic properties for specific applications, topological defects has been introduced to change the chirality of a tube [13]. Theoretical studies have predicted that the presence of heteroatoms can generate pentagon-heptagon defects, thus causing structural reorganization and the formation of stable bends within CNTs [40,41]. A pentagon-heptagon defect pair changes the chirality of a nanotube by one unit from (n, m) to ($n \pm 1$, $m \mp 1$) [42]. Figure 1.2 shows an (8,0) tube joined to a (7,1) tube. The highlighted atoms comprise the defect.

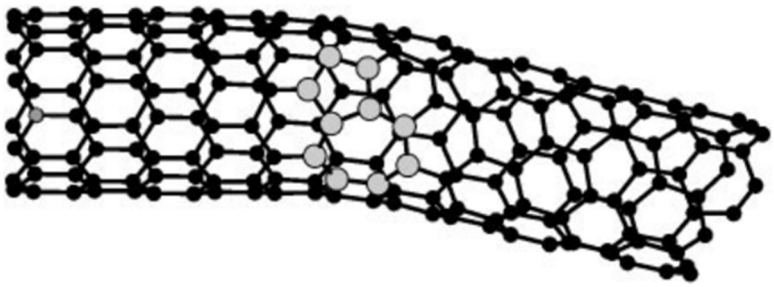

Figure 1.2 Atomic structure of an (8, 0) tube joined to a (7,1) tube. The large light-grey balls denote the atoms forming the heptagon-pentagon pair [42].

To effective tailor the properties of CNTs, different atoms (doping) has been used into a CNT lattice to alter its structure and properties [43]. The presence of heteroatoms, including boron, chlorine, nitrogen, and sulfur, are able to induce

dramatic tubule morphology changes in CNTs, such as nanoscale multijunctions [12,40,44–46]. Figure 1.3 shows a (5,5)/(9,0) CNT modified with the sulfur atoms.

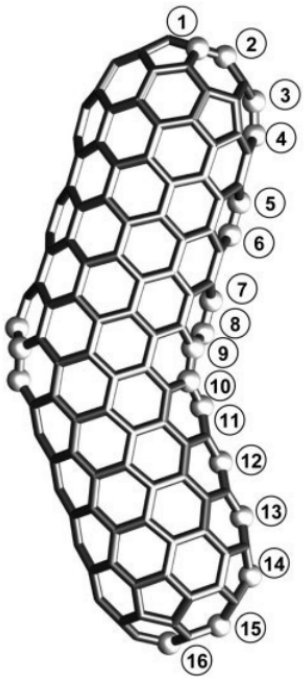

Figure 1.3 Optimized structure for a hybrid (5,5)/(9,0) capped CNT. The positions for atom substitution are marked [43].

1.3.2 Carbon Nanotube Morphology

Figure 1.4a shows a transmission electron microscope (TEM) image showing the nanostructure of a MWNT where several layers of graphitic carbon and a hollow core are evident. MWNTs are essentially concentric SWNTs. These concentric nanotubes are held together through van der Waals bonding. Figure 1.4b shows the cross-sectional SEM image of 3D CNT sponge with self-assembled and randomly entangled MWNTs [10].

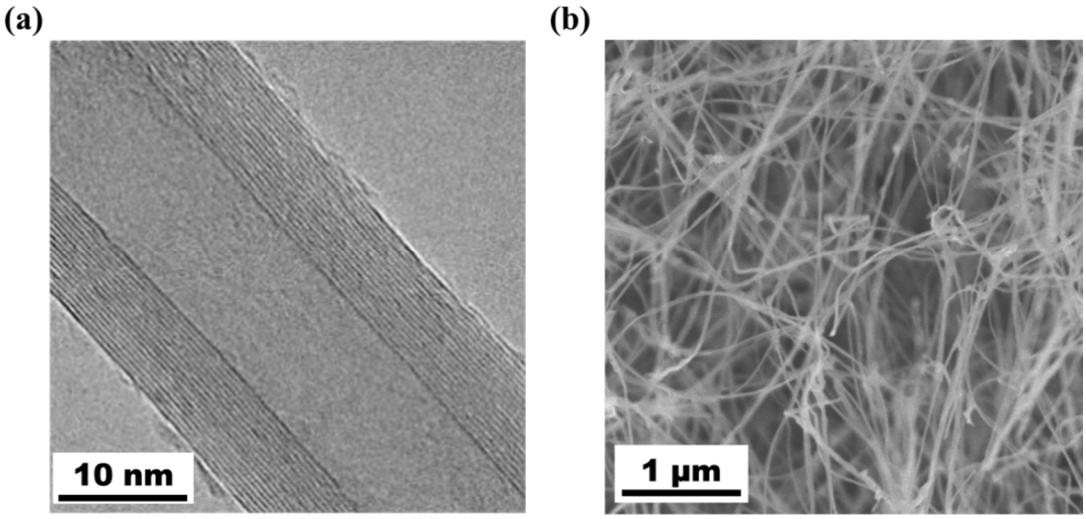

Figure 1.4 (a) High resolution TEM image of MWCNT, showing the graphite layers and concentric structure [47]. (b) Cross-sectional SEM image of a 3D undoped-MWNT sponge showing a porous morphology and overlapped CNTs.

With the introduced defect into the hexagonal carbon network, the straight tubular morphology of pristine CNT would be permanently changed. The pentagon-heptagon defects results in the stable bends in MWNTs [41] which are found to be continuous and somewhat periodic along the tube length. Figure 1.5 shows the high resolution TEM and SEM image of CBxMWNT and its porous network. The entangled CBxMWNT is fabricated via boron doping strategy via chemical vapor deposition methods. The boron dopant is found to favor the zigzag chirality and catalyze the growth of these long, entangled and novel sponge-like structures.

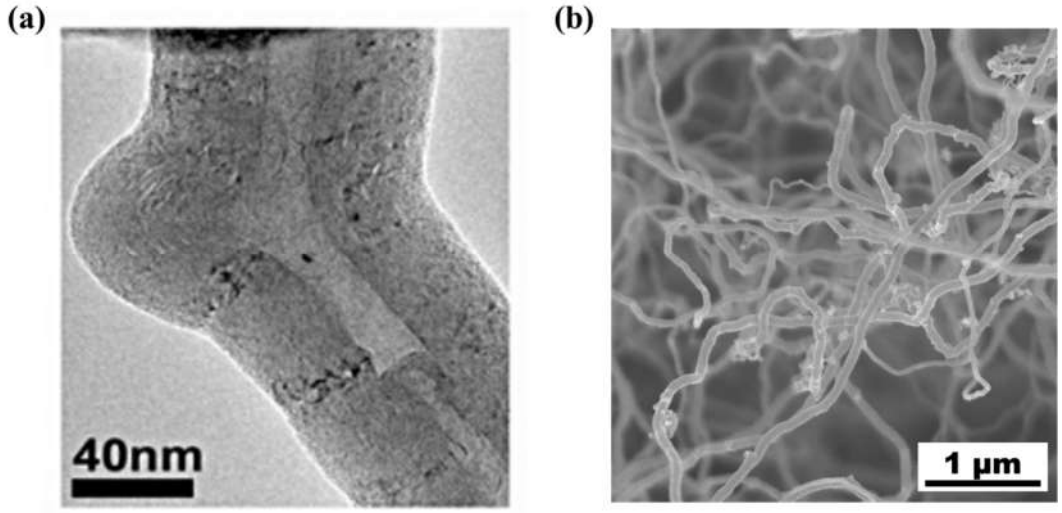

Figure 1.5 (a) High resolution TEM image of CBxMWNT, showing the "elbow" defects [13]. (b) Cross-sectional SEM image of a 3D CBxMWNT sponge showing a randomly oriented and entangled CNTs with "elbow" junctions.

1.4 Mechanical Characterization and Modeling of 3D Carbon Nanotubes

To better understand the mechanical properties of CNTs, a number of investigators have attempted to characterize CNTs directly. The Young's modulus of MWCNT was initially estimated in transmission electron microscope (TEM) by measuring its thermal vibration amplitude and was averaged at 1.8 TPa [16]. Direct measurement by atomic-force microscope (AFM) was performed. By analyzing the force versus displacement characteristics, the Young's modulus of MWCNT was estimated at 1.28 TPa [48]. Nanoindentation method was also applied on the CNT forests to identify effective modulus of individual MWNT [49]. During the nanoindentation experiments, an indenter tip is driven into and then withdrawn from a specimen. The elastic properties were than deduced from nanoindentation force-penetration depth curves. The effective modulus of MWNT was estimated at 0.91~1.24 TPa. In additional to previous studies which simply reveals the elastic

properties of MWNT with “defect-free” morphology, Poncharal found that the modulus of MWNT would decrease sharply (from about 1 to 0.1 TPa) with increasing diameter (from 8 to 40 nanometers) in TEM measurement, which indicates the potential wavelike distortions in the nanotubes with larger diameter and number of graphite layers [50]. For MWNT with high defect ratio, the Young’s modulus was measured as low as ~10 GPa [51]. In additional to the exceptionally high modulus, the reported tensile strength of CNT ranges from 13 to 150 GPa, which is shown to be much higher than that of high-strength steel (2 GPa) [52]. Theoretical studies were also performed to predict the modulus of CNTs [53–55]. Lu conducted a comprehensive study on the elastic properties of single walled nanotubes using an empirical lattice dynamical model. It was predicted that the CNTs are as strong as diamond, of which the Young’ modulus is ~1 TPa. Lu considered that the elastic moduli are insensitive to the CNTs’ diameter and structure, such as helicity, tube radius and number of layers [54]. Li and Chou investigated the elastic properties of MWCN by molecular structural mechanics methods. The nested individual layers of an MWNT were treated as single-walled frame-like structures. The computational results showed that the Young's moduli of MWCNTs are in the ranges of 1.05±0.05. But unlike Lu, they found that the tube diameter, tube chirality and number of tube layers have some noticeable effects on the elastic properties of MWNTs [56].

The collective mechanical properties of CNTs were extensively studied as well, however, the characterization results were found to be remarkable difference from that of individual CNTs. For instance, Yu *et al.* investigated the tensile properties of MWNT bundles by AFM and the experimentally calculated modulus ranges from 0.3 to 1 TPa [22]. Intertube slippage was observed during the tensile loading which

lead to the failure and lower modulus of MWNT. The moduli of vertically aligned CNTs (VACNT) characterized by compression testing fall in the range of a few kPa, which was several order less than that of individual CNTs [57–59].

Besides investigating stiffness and strength, more studies have been focusing on the viscoelastic properties of CNT assemblies due to energy loss observed during cyclic loading [10,11,57,60]. Studies have shown that the viscoelastic behavior of CNT materials is influenced by a number of factors. Pathak *et al.* confirmed that faster loading rate would lead to larger hysteresis on VACNT [60]; Lattanzi *et al.* studied the nonlinear viscoelasticity of VACNT and found that stress relaxation rate is dependent on the compressive strain level [61]. Zhang *et al.* reported the creep behavior of VACNT under a nano-indenter [62]. They found that CNT array's strain rate sensitivity decreases with the increasing density. Therefore, different structure/morphology of nanotubes, which are determined by fabrication conditions, could lead to their scattering mechanical properties of CNTs and their assemblies.

Few comprehensive studies have been done on compressive behavior of 3D CNT structures, especially for their structure/property relationship. To expand the application of 3D CNT, it is indispensable and necessary to reveal and understand the mechanical properties of 3D CNTs first, especially the collective behavior in nanotube assemblies and the relationship between microstructure/morphology and the mechanical properties of CNT structures.

1.5 Mechanical Properties of Carbon Nanotube Based Composites

The preliminary research on CNTs reveals the outstanding mechanical properties of CNTs, including stiffness and strength, provides us the fundamental knowledge of the mechanical response of CNTs and consequently stimulates the

development of CNT-reinforce composites for both structural and functional applications, especially for their excellent strength and stiffness properties.

In general, the most common method for fabricating CNT polymer composites is based on solution processing. The process is divided into three stage: dispersing CNTs in either a solvent or polymer solution by agitation, mixing the nanotubes and polymer evenly, evaporation of the solvent to form composites [63]. The critical issue of the method is the efficient dispersion of nanotubes in the relevant solvent, which can be achieved by bath or tip sonication [64].

Chou *et al.* reviewed the recent advantage composites reinforced with different hierarchical structural of CNTs. They summarized that the addition of CNTs would improves the elastic modulus, strength, and fracture toughness of the polymeric matrices, especially at low CNT loadings. The fatigue life of glass/epoxy composites would also be improved by introduction CNTs as fillers [65]. For example, Gojny *et al.* characterized MWNT/epoxy resin composites, with only the addition of 1 wt%, they achieved 6% increase in the stiffness and a 23% increase in the fracture toughness without any sacrifice in the other properties [66]. Ogasawara *et al.* fabricated a phenylethyl composites with 3.3wt% MWNT, the resulting elastic modulus have around 10% increase, however the consequence strength reduced [67]. Qian *et al.* characterized the mechanical properties of CNT/polystyrene composites. Around 36 - 42% increase in the elastic stiffness and a 25% increase in the tensile strength was observed [68].

It was considered that the limited lengths and the random distribution of CNTs inside the composites are not the best for high strength structural composites which require loads to be carried by continuous fibers across the dimensions of the composite

structures [21]. With the successful manufacture of millimeter long CNTs [69], more research interests were transferred to fabricate and characterize the composites with continuous CNTs. The unconfined compression tests on VACNT composites showed tremendous improvement in the longitudinal modulus (up to 3300%) as well as damping capability (up to 2100%) [21]. Meanwhile, extensive studies on VACNT composites revealed their viscoelasticity, excellent fatigue resistance, and outstanding mechanical resilience [21,70,71]. The extraordinary properties of VACNT suggest that properly engineered continuous CNT composite structures could have more applications including biomedical engineering and military materials.

1.6 Summary

The exceptional mechanical properties demonstrated for the CNTs, with the development of its engineered 3D structure, make this new form of carbon an excellent candidate for wider application. Before these extraordinary properties observed at the 1D or 2D scale are realized in all the dimensions, considerable basic research is necessary. Full understanding of the mechanical behavior of 3D CNTs, requires knowledge of the elastic properties of junctions as well as the influence of junction-related morphologies to the mechanical behavior of bulk CNTs and their composites . Although this requirement is no different from that in the conventional CNTs which is straight along their length, the "elbow-like" or covalent junctions on the 3D CNTs poses new challenges in the mechanical characterization and modeling. Preliminary theoretical research in 3D CNTs indicated their potential in reinforcement, viscoelastic and environmental application. Fundamental work in characterization,

analysis and modeling is crucial before the structural and functional properties of this cutting-edge materials can be optimized.

REFERENCES

[1] D. Qian, G.J. Wagner, W.K. Liu, M.-F. Yu, R.S. Ruoff, Mechanics of carbon nanotubes, Appl. Mech. Rev. 55 (2002) 495–532.

[2] B.I. Yakobson, P. Avouris, Mechanical Properties of Carbon Nanotubes, Carbon Nanotub. 327 (2001) 287–327.

[3] P. Ajayan, O. Zhou, Applications of carbon nanotubes, Carbon Nanotub. 425 (2001) 391–425.

[4] M.F.L. De Volder, S.H. Tawfick, R.H. Baughman, A.J. Hart, Carbon Nanotubes: Present and Future Commercial Applications, Sci. . 339 (2013) 535–539.

[5] E.H.T. Teo, W.K.P. Yung, D.H.C. Chua, B.K. Tay, A Carbon Nanomattress: A New Nanosystem with Intrinsic, Tunable, Damping Properties, Adv. Mater. 19 (2007) 2941–2945.

[6] M.A. Worsley, S.O. Kucheyev, J.H. Satcher, A. V Hamza, T.F. Baumann, Mechanically robust and electrically conductive carbon nanotube foams, Appl. Phys. Lett. 94 (2009).

[7] S. Nardecchia, D. Carriazo, M.L. Ferrer, M.C. Gutierrez, F. del Monte, Three dimensional macroporous architectures and aerogels built of carbon nanotubes and/or graphene: synthesis and applications, Chem. Soc. Rev. 42 (2013) 794–830.

[8] J.M. Romo-Herrera, M. Terrones, H. Terrones, S. Dag, V. Meunier, Covalent 2D and 3D Networks from 1D Nanostructures: Designing New Materials, Nano Lett. 7 (2006) 570–576.

[9] J.-Q. Huang, Q. Zhang, M.-Q. Zhao, G.-H. Xu, F. Wei, Patterning of hydrophobic three-dimensional carbon nanotube architectures by a pattern transfer approach, Nanoscale. 2 (2010) 1401–1404.

[10] X. Gui, J. Wei, K. Wang, A. Cao, H. Zhu, Y. Jia, et al., Carbon nanotube sponges., Adv. Mater. 22 (2010) 617–21.

[11] X. Gui, A. Cao, J. Wei, H. Li, Y. Jia, Z. Li, et al., Soft, Highly Conductive Nanotube Sponges and Composites with Controlled Compressibility, ACS Nano. 4 (2010) 2320–2326.

[12] C. Shan, W. Zhao, X.L. Lu, D.J. O'Brien, Y. Li, Z. Cao, et al., Three-dimensional nitrogen-doped multiwall carbon nanotube sponges with tunable properties, Nano Lett. 13 (2013) 5514–5520.

[13] D.P. Hashim, N.T. Narayanan, J.M. Romo-Herrera, D. a. Cullen, M.G. Hahm, P. Lezzi, et al., Covalently bonded three-dimensional carbon nanotube solids via boron induced nanojunctions, Sci. Rep. 2 (2012).

[14] S. Ozden, T.N. Narayanan, C.S. Tiwary, P. Dong, A.H.C. Hart, R. Vajtai, et al., 3D Macroporous Solids from Chemically Cross-linked Carbon Nanotubes, Small. 11 (2015) 688–693.

[15] S. Ozden, C.S. Tiwary, A.H.C. Hart, A.C. Chipara, R. Romero-Aburto, M.-T.F. Rodrigues, et al., Density Variant Carbon Nanotube Interconnected Solids, Adv. Mater. 27 (2015) 1842–1850.

[16] M.M.J. Treacy, T.W. Ebbesen, J.M. Gibson, Exceptionally high Young's modulus observed for individual carbon nanotubes, Nature. 381 (1996) 678–680.

[17] J.-P. Salvetat, G.A.D. Briggs, J.-M. Bonard, R.R. Bacsa, A.J. Kulik, T. Stöckli, et al., Elastic and Shear Moduli of Single-Walled Carbon Nanotube Ropes, Phys. Rev. Lett. 82 (1999) 944–947.

[18] M.R. Falvo, G.J. Clary, R.M. Taylor II, V. Chi, F.P. Brooks Jr., S. Washburn, et al., Bending and buckling of carbon nanotubes under large strain, Nature. 389 (1997) 582–584.

[19] S. Iijima, Helical microtubules of graphitic carbon, Nature. 354 (1991) 56–58.

[20] E.T. Thostenson, Z. Ren, T.-W. Chou, Advances in the science and technology of carbon nanotubes and their composites: a review, Compos. Sci. Technol. 61 (2001) 1899–1912.

[21] L. Ci, J. Suhr, V. Pushparaj, X. Zhang, P.M. Ajayan, Continuous Carbon Nanotube Reinforced Composites, Nano Lett. 8 (2008) 2762–2766.

[22] M.-F. Yu, O. Lourie, M.J. Dyer, K. Moloni, T.F. Kelly, R.S. Ruoff, Strength and Breaking Mechanism of Multiwalled Carbon Nanotubes Under Tensile Load, Sci. . 287 (2000) 637–640.

[23] M.-F. Yu, B.S. Files, S. Arepalli, R.S. Ruoff, Tensile Loading of Ropes of Single Wall Carbon Nanotubes and their Mechanical Properties, Phys. Rev. Lett. 84 (2000) 5552–5555.

[24] P.G. Collins, P. Avouris, Nanotubes for Electronics, Sci. Am. 283 (2000) 62–69.

[25] S. Iijima, C. Brabec, A. Maiti, J. Bernholc, Structural flexibility of carbon nanotubes, J. Chem. Phys. 104 (1996) 2089–2092.

[26] W. Bauhofer, J.Z. Kovacs, A review and analysis of electrical percolation in carbon nanotube polymer composites, Compos. Sci. Technol. 69 (2009) 1486–1498.

[27] A.E. Aliev, J. Oh, M.E. Kozlov, A.A. Kuznetsov, S. Fang, A.F. Fonseca, et al., Giant-Stroke, Superelastic Carbon Nanotube Aerogel Muscles, Sci. . 323 (2009) 1575–1578.

[28] L. Xiao, Z. Chen, C. Feng, L. Liu, Z.-Q. Bai, Y. Wang, et al., Flexible, Stretchable, Transparent Carbon Nanotube Thin Film Loudspeakers, Nano Lett. 8 (2008) 4539–4545.

[29] A. Cao, P.L. Dickrell, W.G. Sawyer, M.N. Ghasemi-Nejhad, P.M. Ajayan, Super-Compressible Foamlike Carbon Nanotube Films, Sci. . 310 (2005) 1307–1310.

[30] S. Timur, U. Anik, D. Odaci, L. Gorton, Development of a microbial biosensor based on carbon nanotube (CNT) modified electrodes, Electrochem. Commun. 9 (2007) 1810–1815.

[31] S. Agnihotri, M. Rostam-Abadi, ENERGY AND ENVIRONMENTAL APPLICATIONS OF CARBON NANOTUBES, Fuel Chem. Div. Prepr. 47 (2002) 476.

[32] S. Kabiri, D.N.H. Tran, T. Altalhi, D. Losic, Outstanding adsorption performance of graphene–carbon nanotube aerogels for continuous oil removal, Carbon N. Y. 80 (2014) 523–533.

[33] R.R. Kohlmeyer, M. Lor, J. Deng, H. Liu, J. Chen, Preparation of stable carbon nanotube aerogels with high electrical conductivity and porosity, Carbon N. Y. 49 (2011) 2352–2361.

[34] M. Crespo, M. González, A.L. Elías, L. Pulickal Rajukumar, J. Baselga, M. Terrones, et al., Ultra-light carbon nanotube sponge as an efficient electromagnetic shielding material in the GHz range, Phys. Status Solidi – Rapid Res. Lett. 8 (2014) 698–704.

[35] X. Gui, A. Cao, J. Wei, H. Li, Y. Jia, Z. Li, et al., Soft, highly conductive nanotube sponges and composites with controlled compressibility, ACS Nano. 4 (2010) 2320–2326.

[36] Y. Wu, N. Yi, L. Huang, T. Zhang, S. Fang, H. Chang, et al., Three-dimensionally bonded spongy graphene material with super compressive elasticity and near-zero Poisson's ratio, Nat Commun. 6 (2015).

[37] Z. Zeng, X. Gui, Z. Lin, L. Zhang, Y. Jia, A. Cao, et al., Carbon Nanotube Sponge-Array Tandem Composites with Extended Energy Absorption Range, Adv. Mater. (2012) n/a–n/a.

[38] Functionalization of Nanotube Surfaces, http://what-when-how.com/nanoscience-and-nanotechnology/functionalization-of-nanotube-surfaces-part-1-nanotechnology/.

[39] T.W. Ebbesen, P.M. Ajayan, Large-scale synthesis of carbon nanotubes, Nature. 358 (1992) 220–222.

[40] M.U. Kahaly, Defect states in carbon nanotubes and related band structure engineering: A first-principles study, J. Appl. Phys. 105 (2009).

[41] B. Dunlap, Connecting carbon tubules, Phys. Rev. B. 46 (1992) 1933–1936.

[42] L. Chico, V. Crespi, L. Benedict, S. Louie, M. Cohen, Pure Carbon Nanoscale Devices: Nanotube Heterojunctions, Phys. Rev. Lett. 76 (1996) 971–974.

[43] B.G. Sumpter, J. Huang, V. Meunier, J.M. Romo-Herrera, E. Cruz-Silva, H. Terrones, et al., A theoretical and experimental study on manipulating the structure and properties of carbon nanotubes using substitutional dopants, Int. J. Quantum Chem. 109 (2009) 97–118.

[44] J.M. Romo-Herrera, B.G. Sumpter, D.A. Cullen, H. Terrones, E. Cruz-Silva, D.J. Smith, et al., An Atomistic Branching Mechanism for Carbon Nanotubes: Sulfur as the Triggering Agent, Angew. Chemie Int. Ed. 47 (2008) 2948–2953.

[45] J.M. Romo-Herrera, D.A. Cullen, E. Cruz-Silva, D. Ramírez, B.G. Sumpter, V. Meunier, et al., The Role of Sulfur in the Synthesis of Novel Carbon Morphologies: From Covalent Y-Junctions to Sea-Urchin-Like Structures, Adv. Funct. Mater. 19 (2009) 1193–1199.

[46] M. Endo, H. Muramatsu, T. Hayashi, Y.-A. Kim, G. Van Lier, J.-C. Charlier, et al., Atomic nanotube welders: Boron interstitials triggering connections in double-walled carbon nanotubes, Nano Lett. 5 (2005) 1099–1105.

[47] Carbon Nanomaterials, (n.d.).

[48] E.W. Wong, P.E. Sheehan, C.M. Lieber, Nanobeam Mechanics: Elasticity, Strength, and Toughness of Nanorods and Nanotubes, Sci. . 277 (1997) 1971–1975.

[49] H.J. Qi, K.B.K. Teo, K.K.S. Lau, M.C. Boyce, W.I. Milne, J. Robertson, et al., Determination of mechanical properties of carbon nanotubes and vertically aligned carbon nanotube forests using nanoindentation, J. Mech. Phys. Solids. 51 (2003) 2213–2237.

[50] P. Poncharal, Z.L. Wang, D. Ugarte, W.A. de Heer, Electrostatic Deflections and Electromechanical Resonances of Carbon Nanotubes, Sci. . 283 (1999) 1513–1516.

[51] J.-P. Salvetat, A.J. Kulik, J.-M. Bonard, G.A.D. Briggs, T. Stöckli, K. Méténier, et al., Elastic Modulus of Ordered and Disordered Multiwalled Carbon Nanotubes, Adv. Mater. 11 (1999) 161–165.

[52] E.T. Thostenson, C. Li, T.W. Chou, Nanocomposites in context, Compos. Sci. Technol. 65 (2005) 491–516.

[53] C. Li, Elastic moduli of multi-walled carbon nanotubes and the effect of van der Waals forces, Compos. Sci. Technol. 63 (2003) 1517–1524.

[54] J.P. Lu, Elastic properties of single and multilayered nanotubes, J. Phys. Chem. Solids. 58 (1997) 1649–1652.

[55] J. Bernholc, C. Brabec, M. Buongiorno Nardelli, A. Maiti, C. Roland, B.I. Yakobson, Theory of growth and mechanical properties of nanotubes, Appl. Phys. A. 67 (1998) 39–46.

[56] C. Li, T.-W. Chou, Multiscale modeling of compressive behavior of carbon nanotube/polymer composites, Compos. Sci. Technol. 66 (2006) 2409–2414.

[57] A. Cao, P.L. Dickrell, W.G. Sawyer, M.N. Ghasemi-Nejhad, P.M. Ajayan, Super-compressible foamlike carbon nanotube films., Science. 310 (2005) 1307–10.

[58] T. Tong, Y. Zhao, L. Delzeit, A. Kashani, M. Meyyappan, A. Majumdar, Height Independent Compressive Modulus of Vertically Aligned Carbon Nanotube Arrays, Nano Lett. 8 (2008) 511–515.

[59] C.P. Deck, J. Flowers, G.S.B. McKee, K. Vecchio, Mechanical behavior of ultralong multiwalled carbon nanotube mats, J. Appl. Phys. 101 (2007) -.

[60] S. Pathak, E.J. Lim, P. Pour Shahid Saeed Abadi, S. Graham, B.A. Cola, J.R. Greer, Higher Recovery and Better Energy Dissipation at Faster Strain Rates in Carbon Nanotube Bundles: An in-Situ Study, ACS Nano. 6 (2012) 2189–2197.

[61] Nonlinear viscoelasticity of freestanding and polymer-anchored vertically aligned carbon nanotube foams, J. Appl. Phys. 111 (2012) 74314.

[62] Q. Zhang, Y.C. Lu, F. Du, L. Dai, J. Baur, D.C. Foster, Viscoelastic creep of vertically aligned carbon nanotubes, J. Phys. D. Appl. Phys. 43 (2010).

[63] J.N. Coleman, U. Khan, W.J. Blau, Y.K. Gun'ko, Small but strong: A review of the mechanical properties of carbon nanotube–polymer composites, Carbon N. Y. 44 (2006) 1624–1652.

[64] Z. Spitalsky, D. Tasis, K. Papagelis, C. Galiotis, Carbon nanotube–polymer composites: Chemistry, processing, mechanical and electrical properties, Prog. Polym. Sci. 35 (2010) 357–401.

[65] T.-W. Chou, L. Gao, E.T. Thostenson, Z. Zhang, J.-H. Byun, An assessment of the science and technology of carbon nanotube-based fibers and composites, Compos. Sci. Technol. 70 (2010) 1–19.

[66] F.H. Gojny, M.H.G. Wichmann, U. Köpke, B. Fiedler, K. Schulte, Carbon nanotube-reinforced epoxy-composites: enhanced stiffness and fracture toughness at low nanotube content, Compos. Sci. Technol. 64 (2004) 2363–2371.

[67] T. Ogasawara, Y. Ishida, T. Ishikawa, R. Yokota, Characterization of multi-walled carbon nanotube/phenylethynyl terminated polyimide composites, Compos. Part A Appl. Sci. Manuf. 35 (2004) 67–74.

[68] D. Qian, E.C. Dickey, R. Andrews, T. Rantell, Load transfer and deformation mechanisms in carbon nanotube-polystyrene composites, Appl. Phys. Lett. 76 (2000) 2868–2870.

[69] X. Zhang, A. Cao, B. Wei, Y. Li, J. Wei, C. Xu, et al., Rapid growth of well-aligned carbon nanotube arrays, Chem. Phys. Lett. 362 (2002) 285–290.

[70] J. Suhr, P. Victor, L. Ci, S. Sreekala, X. Zhang, O. Nalamasu, et al., Fatigue resistance of aligned carbon nanotube arrays under cyclic compression., Nat. Nanotechnol. 2 (2007) 417–421.

[71] M. Zhang, K.R. Atkinson, R.H. Baughman, Multifunctional Carbon Nanotube Yarns by Downsizing an Ancient Technology, Sci. . 306 (2004) 1358–1361.

Chapter 2

CONTROLLABLE AND PREDICTABLE VISCOELASTIC BEHAVIOR OF 3D BORON-DOPED MULTIWALLED CARBON NANOTUBE SPONGES

2.1 Introduction

Carbon nanotubes (CNTs) and graphene possess outstanding mechanical, electrical and thermal properties [1–3]. However, translation of such extraordinary properties into real-world applications remains challenging. CNT architectures, an ensemble of individual nanotubes, have been widely explored for their potential use in various areas [4–7]. With recent technical advances in nanotube synthesis, such as chemical vapor deposition and solution chemistry techniques, there is a rapidly growing interest in macro-scale three dimensional (3D) nanotube architectures [8–11]. In contrast to vertically aligned nanotube arrays, randomly networked and sponge-like 3D architectures can be considered isotropic and homogeneous. Formed with randomly and highly entangled nanotube networks, CNT aerogels have been synthesized in a number of studies [8,12–14]. Covalently bonded 3D hierarchical CNT sponges have been successfully fabricated as well [9–11]. In the 3D sponges with covalent bonds, CNTs can function as "building blocks" and be "welded" together with molecular junctions [15–17]. Hashim et al. used boron as a dopant in CNTs and successfully created "elbow-like" covalent junctions to build 3D hierarchical CNT sponges [10]. Shan et al. synthesized 3D nitrogen-doped CNT sponges by doping both nitrogen and sulfur into CNTs [11]. Given that various 3D CNT structures have been recently fabricated, it is necessary to characterize the macro (or apparent) mechanical properties of 3D CNT architectures and to identify the beneficial effects of transferring the extraordinary properties of nanotubes from one-dimension to 3D architectures. However, there is currently little knowledge on the mechanical behavior

of 3D CNT sponges and the impact of CNT covalent interconnections. We hypothesize that, if engineered and optimized properly, the covalently bonded junctions could serve as an essential structural element to provide controllable properties as well as structural reliability to the porous 3D CNT sponges.

This study investigates the mechanical behavior of 3D CNT sponges, including monotonic stress-strain and viscoelastic properties under compression, with an emphasis on the role of covalent junctions between nanotubes. Materials of interest include 3D boron-doped multiwalled carbon nanotube sponges (CBxMWNT) with elbow-like junctions as well as 3D non-covalent multiwalled carbon nanotube sponges (undoped-MWNT), created via random and entangled nanotube networks [10,13]. Using both a custom-built micro-compression apparatus and a commercial dynamic mechanical analyzer (DMA), the plastic deformation and static and dynamic viscoelastic properties of both CBxMWNT and undoped-MWNT sponges were measured. Comparing of the results of the two materials provides information regarding structure-function relationship for 3D MWNT sponges and offers insight into the role that covalent junctions play in the mechanical behavior of the CBxMWNT sponges. The static viscoelastic properties were quantitatively characterized by coupling stress-relaxation tests with the standard linear solid modeling [18]. Both frequency and temperature sweep testing were performed using DMA. The CBxMWNT sponges with elbow-like junctions and nanotube interconnections exhibited density-dependent behavior in both the static and dynamic viscoelastic tests, while the response of the undoped-MWNT sponges was not related to density and presented a much larger plastic deformation. It should be noted that the density-dependent viscoelastic behavior of the CBxMWNT sponges is predicted, thus

suggesting that 3D CNT sponges with atomic covalent junctions have a great potential in the development of artificial biomaterials, vibrational isolators, and micro-devices with precise controls [19]. To the best of the authors' knowledge, the density-dependent viscoelastic properties of 3D CNT structures have not been previously reported in the literature.

2.2 Synthesis of 3D CNT Sponges

Both CBxMWNT and undoped-MWNT sponges were fabricated according to previous reports [8,10]. In brief, CBxMWNT sponges were grown onto the walls of a quartz tube furnace using ferrocene, toluene, and triethylborane under Ar gas at 860oC via an aerosol assisted catalytic chemical vapor deposition (CVD) method [10]. The undoped-MWNT sponges were synthesized using ferrocene and 1, 2-dichlorobenzene under Ar/H2 gas at 860oC by the CVD method [8].

2.2.1 Mechanical Characterization of CNT Sponges

2.2.1.1 Sample Preparation

Both CB_xMWNT and undoped-MWNT sponges samples were cut into 3 mm diameter cylinders using a Harris Micro-Punch (Ted Pella, INC.). The thickness of the samples ranged from 0.6 to 1.5 mm. For sufficient statistical power, eleven CB_xMWNT and undoped-MWNT samples were prepared and tested.

2.2.1.2 Plastic Deformation

Before testing viscoelastic properties, the plastic deformation of each CNT sponge sample was measured after compression to 60% strain, beyond the purely elastic region. The cylindrical sample was mounted on a DMA (Q800, TA

Instruments) fitted with 15 mm diameter platens at room temperature. An initial preload of 0.01 N was applied to the CBxMWNT sponges in order to provide full contact between the loading platen and sample surface. The preload on the undoped-MWNT samples was adjusted to 0.02 N, according to their greater stiffness. The initial thickness of the sample, $L_{initial}$, was determined as the distance between two platens with 0.02 N preload. Samples were compressed with 60% strain, which was held for 1 hour. Both types of sponges deformed uniformly under the large strain. The thickness after plastic deformation, $L_{deformed,}$ was measured again 24 hours after the force release, sufficient time for the sample to recover according to its intrinsic viscosity. The plastic deformation was defined and calculated as $(L_{initial}-L_{deformed})/L_{initial}$.

2.2.1.3 Stress Relaxation Test and Viscoelastic Model

Stress relaxation tests were conducted with a custom-built compression apparatus. The CNT sponge samples were fixed between two cylindrical indenters with smooth flat ends. The diameter for the cylindrical indenter is 5mm. A 0.01 N preload was applied on the CB_xMWNT sample to ensure full contact between the sponge and indenters. The preload on the undoped-MWNT samples was adjusted to 0.02 N according to their higher stiffness. The original length of the CNT sponge sample, L_r, was measured under the preload. During the stress relaxation test, a constant step displacement (product of L_r and the targeted strain) was applied on the sample and held for 30 minutes. The responsive force of the sample was recorded. The relaxation tests were performed at strain levels of 60%, 50%, 40% and 30% in sequence. Samples were also tested in a random sequence, and no significant

difference was detected between the two protocols. The interval time between tests was 30 minutes, which allowed for the sample's recovery to its original length.

The recorded stress-relaxation curves of each sample were fitted with a standard linear solid model [18], $\text{stress} = (E_1 + E_2 \cdot e^{\frac{-t}{\tau}}) \cdot \text{strain}$, using MATLAB (MathWorks, Inc.). The viscoelastic properties, including equilibrium compressive modulus, E_1, viscous modulus, E_2, and relaxation time, τ, were determined from the curve fitting.

2.2.1.4 DMA Test

The experimental protocol for measuring sample length with the DMA was the same as that of the plastic deformation measurement (see "Plastic Deformation Measurement"). After measuring the initial length of the sponges under the preload, samples were compressed to the desired mean strain (20%, 30%, 40%, or 50%). The sponges were then cyclically compressed and released along their length at constant 1% strain amplitude. The linear viscoelastic range for both sponges was experimentally determined as 1% strain. Frequency sweep tests were run at multi-frequency mode from 0.1 Hz to 10 Hz.

2.2.1.5 Density Measurement

An XP6 microbalance (Mettler-Toledo, Inc.) was used to measure the weight (W) of each CNT sample. The apparent density (ρ) was calculated as $\frac{4W}{\pi d^2 L}$, where d is the sample diameter (3mm) and L is the original length. The original length for the same sample was determined at the beginning of each measurement, and they are denoted as $L_{initial}$, L_r and L_d for plastic deformation, stress relaxation, and DMA tests, respectively.

2.2.2 Statistical Analysis

Student's t-test was used to seek significant differences in properties (plastic deformation, density normalized loss factor) between CB_xMWNT and undoped-MWNT sponges. To detect the correlation between the sponges' viscoelastic properties (equilibrium modulus, viscous modulus, relaxation time, storage modulus, loss modulus, and loss factor) and the apparent density, linear regression analysis was performed. Outlying experimental data was eliminated for each test and the statistical significance was defined as $P<0.05$.

2.3 Results and Discussion

The structural morphologies of CBxMWNT and undoped-MWNT sponges (see Experimental Section for synthesis of both 3D CNT sponges) were examined by scanning electron microscopy (SEM). Figure 2.1a and b show the entangled nature of the CBxMWNT sponges, with elbow-like junctions clearly visible; CNT covalent junctions in these samples have also been observed and reported [10]. In contrast, Figure 2.1c and d indicate that CNTs in undoped-MWNT sponge are mostly straight along their length, with no apparent junctions. The average diameters of the undoped-MWNTs and CBxMWNT, as measured from SEM images, are about 20 nm and 70 nm, respectively.

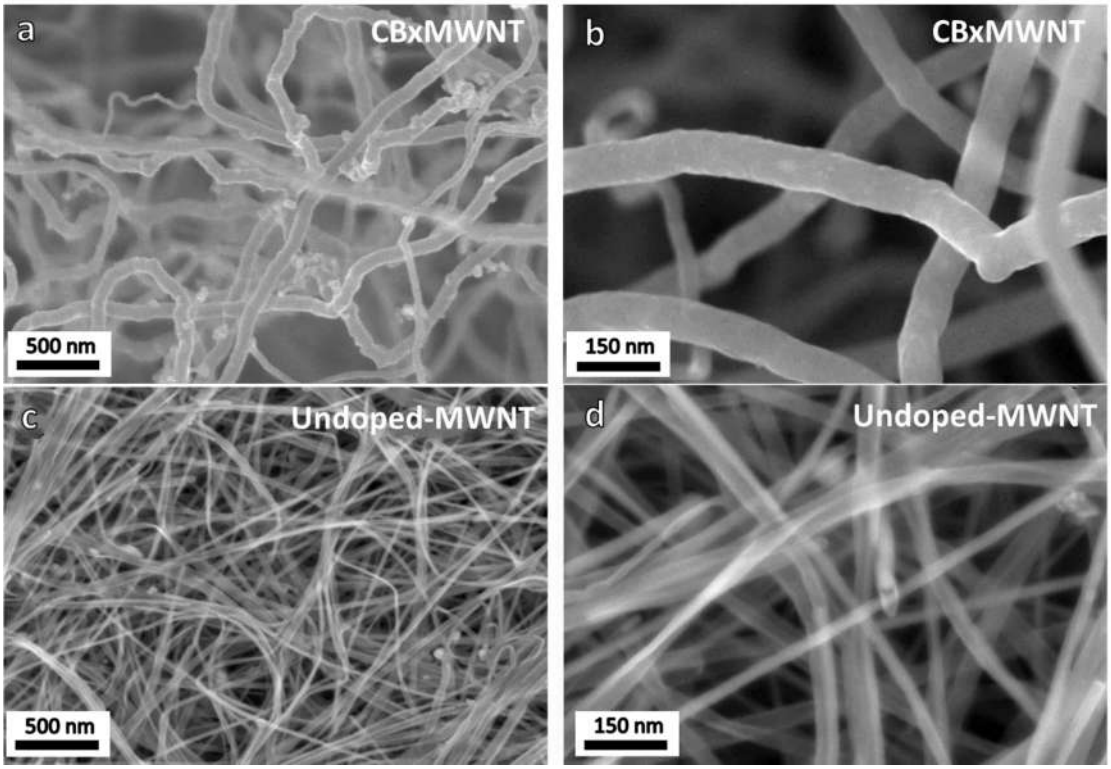

Figure 2.1 SEM images of the as-grown sponges. (a, b) Micrographs showing the morphology of CB_xMWNT sponges and (c, d) undoped-MWNT sponges.

Plastic deformation represents a material's irreversible deformation under mechanical or thermal loading, and is a key criterion in assessing a material's functional capability, particularly for as-grown MWNT sponges with high porosity. A 60% compressive strain was applied to a cylindrical MWNT sponge immediately after fabrication in order to determine the plastic deformation. Experimental details can be found in the Experimental Section. The plastic deformation of the undoped-MWNT sponges was measured to be 12 ± 4.4%, while that of the CBxMWNT sponges was only 5 ± 1.9% (Figure 2.2 a). A student's t-test confirmed the significant difference between the two groups ($P<0.001$) [20], i.e., the plastic deformation of the undoped-

MWNT sponges is larger than that of the CBxMWNT sponges. Considering the composition of random and highly entangled CNTs in undoped-MWNTs, its large plastic deformation under compression may be attributed to a combination of rearrangement, buckling, and aggregation of CNTs [21]. It has been shown that, under compression, the reestablished van der Waals (vdW) forces can often form bundles of CNTs [22]. However, the covalently bonded junctions in the CBxMWNT sponges are able to overcome such vdW forces and enable more complete recovery via a purely elastic mechanism [10]. This resistance to vdW forces may further result in fewer buckled and bundled CNTs inside the structure after a large deformation, thus permitting much less plastic deformation in the CBxMWNT sponges.

The plastic deformation with respect to the density of CBxMWNT and undoped-MWNT sponges is plotted in Figure 2. 2 b. Interestingly, linear regression analysis showed that the undoped-MWNT sponges exhibit a strong relationship between the plastic deformation and density, where the plastic deformation decreases with increasing density. In contrast, the plastic deformation of CBxMWNT sponges is density-independent. As discussed above, the “elbow-like” junctions in the CBxMWNT sponges could endow the material much greater resistance to compressive loading, thereby giving rise to density-independent dimensional recoverability, even at low densities. For undoped-MWNT sponges, as the density increases an increased number of CNTs may participate in recovering their original shape, which at least partially contributes to the density-dependent behavior in plastic deformation.

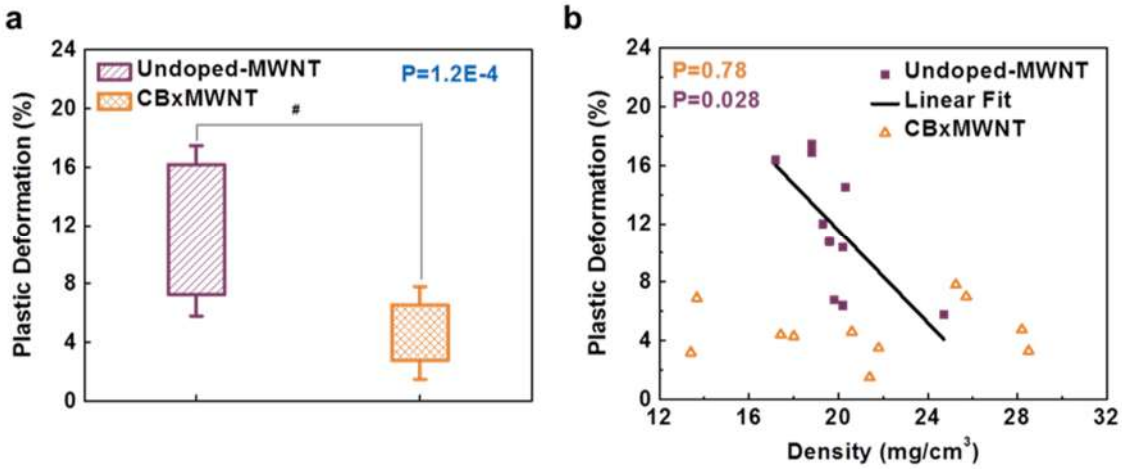

Figure 2.2 **(a) Plastic deformation of CBxMWNT and undoped-MWNT sponges. Plastic deformation for CBxMWNT (n=11) and undoped-MWNT (n=10) represented as a box-and-whisker plot, with the standard definitions. # indicates a significant difference between CBxMWNT and undoped-MWNT sponges (P < 0.001). (b) The plastic deformation of CBxMWNT and undoped-MWNT sponges plotted as a function of density. The black line indicates a significant linear correlation between the plastic deformation and apparent density of the undoped-MWNT sponges (P=0.028). For all plots, statistical significance was indicated by P<0.05.**

The stress-strain relations for both CNT sponges was characterized with quasi-static compressive (1 μm/s) cyclic loadings (loading–unloading). Hysteresis responses in both undoped-MWNT and CBxMWNT sponges were observed in tests, similar to the behaviors reported for a number of CNT structures (Figure 2.3) [19, 23–25]. Cylindrical samples (0.6 to 1.5 mm in thickness) were compressed on a custom-built micro-testing apparatus at 1μm/s loading speed. Undoped-MWNT shows a nearly-linear stress response after 6 loading-unloading cycles, especially at the low strain level (<20%). Plastic deformation shifts the curve along the strain axis. In contrast, the CBxMWNT sponge demonstrates a typical nonlinear stress response with a toe region. The hysteresis cycles shift slightly due to small as-fabricated plastic deformation.

Since the resistance of interstitial air flow to the network deformation is negligible at a quasi-static loading rate (1μm/s), the hysteresis indicates the intrinsic viscous nature of the 3D CNT sponges.

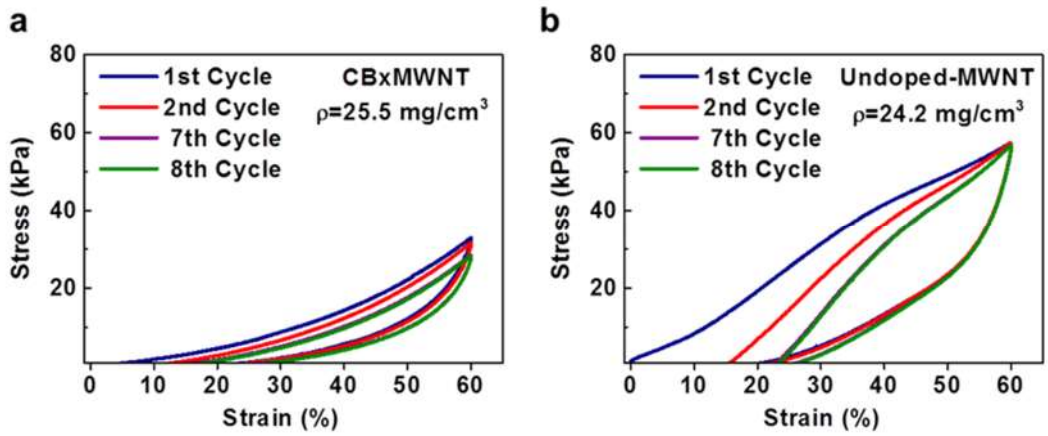

Figure 2.3 Loading and unloading stress-strain curves of as-fabricated undoped-MWNT and CB_xMWNT sponges with similar bulk densities.

The prominent hysteresis behavior motivated a thorough investigation of the viscoelastic characteristics of both CNT sponges. First, a stress relaxation test was performed on two groups of cylindrical samples. A typical stress relaxation response from the CBxMWNT sponge is shown in Figure 2.4a. Under a constant compressive strain (30%), the resistant stress gradually decreases over time and reaches an equilibrium state. A similar stress relaxation response was also noted for the undoped-MWNT sponges. It has been reported that the stress relaxation behavior of the CNT sponges, similar to many other viscoelastic materials, can likely be ascribed to micro-structural reorganizations, which minimize internal stresses and allow the sponge to accommodate the applied load [26]. Moreover, as a typical porous elastic material,

sponges under compression also squeeze air out of their networks as they deform, inducing dissipation of energy and viscoelastic characteristics as a result of friction between the solid and air phases.[27]

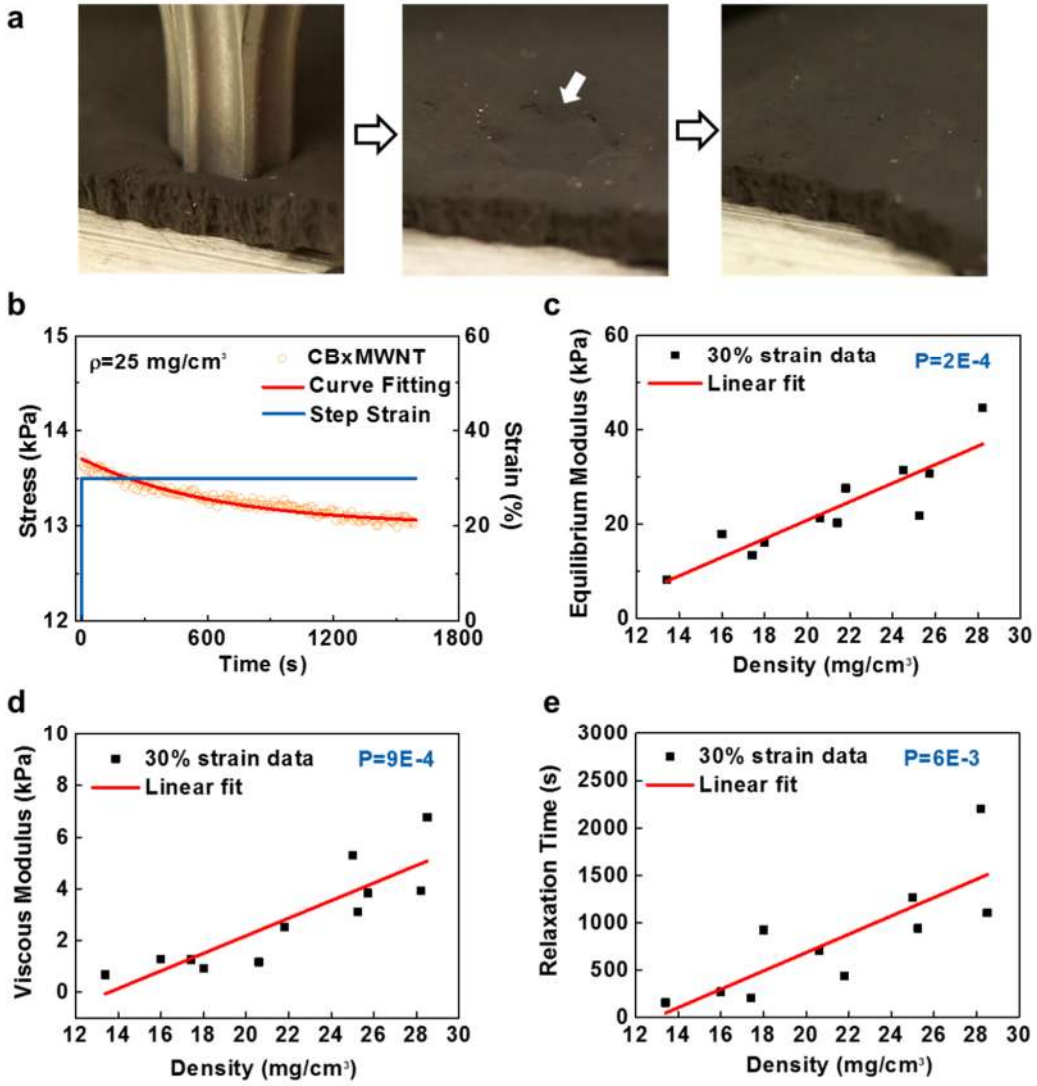

Figure 2.4 **(a) Viscoelastic behavior of CBxMWNT sponge. The sponge was indented within the elastic region, and a noticeable indent (white arrow) was observed immediately after unloading. Deformation almost disappeared a half hour later. (b) A representative stress relaxation response curve for a CB_xMWNT sponge under constant strain deformation. The relaxation response was fitted with standard linear solid model. A similar relaxation response was found for undoped-MWNT sponges as well. (c-e) Equilibrium modulus, viscous modulus, and relaxation time of CB_xMWNT sponges under 30% compressive strain, plotted as a function of sponge density.**

The stress relaxation response, which is often referred to as the static viscoelastic behavior, was quantified for both CNT sponges by employing a standard linear solid model to calculate the equilibrium modulus, viscous modulus, and relaxation time. Given that the viscoelastic characteristics of porous materials are often affected by the porosity (or volume fraction of the solid network) [28], the quantified viscoelastic properties were also correlated with the sponge density. Linear regression analysis showed that the equilibrium modulus, viscous modulus, and relaxation time of the CBxMWNT sponges are all density-dependent (Figure 2.4b-d). In addition, similar correlations confirmed the density dependence at other compressive strain levels, including 40%, 50%, and 60%. Therefore, for the CBxMWNT sponge, all the quantified viscoelastic properties increase with the sponge density. This important observation implies that a higher density in 3D CNT sponges would lead to: 1) greater support from CNT networks with a larger equilibrium modulus; 2) smaller permeability of the sponge, thus resulting in greater frictional forces between the air and CNTs and thus a higher viscous modulus; and 3) increased time required for air to be squeezed out of the network, which corresponds to a longer relaxation time. Importantly, the results reveal that the viscoelastic behavior of the CBxMWNT sponges can be regulated by controlling their densities. This favorable feature may be a beneficial effect resulting from the existence of covalent junctions in the CBxMWNT sponges, which also makes the micro-structural morphology more predictable, regardless of the sponge density, as demonstrated by the small plastic deformation post fabrication. The controllable mechanical properties of 3D CNT sponges are of great practical importance for the design and subsequent broad application of systems utilizing such viscoelastic materials. In sharp contrast to the

behavior of the CBxMWNT sponges, the general viscoelastic behavior of the undoped-MWNT sponges were found to be density-independent at almost all strain levels, except the equilibrium modulus at high strain levels (Figure 2.5). Therefore, the behavior of the undoped-MWNT sponges does not appear to be controllable (to any useful degree) with respect to density. The density-independent viscoelastic responses of the undoped-MWNT sponges might be attributed to significant changes in the micro-structural morphology under a given loading condition, due to the highly uneven aggregation and buckling between nanotubes. The viscoelastic properties for both sponges under different loading condition are summarized in Figure 2.6.

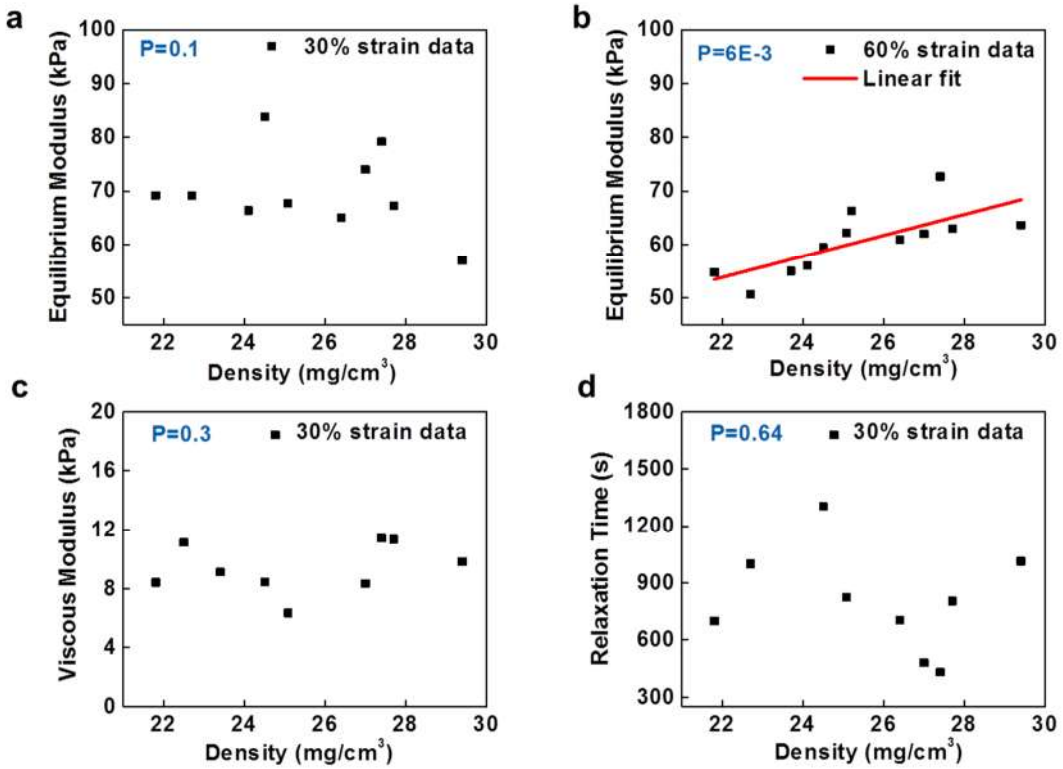

Figure 2.5 **(a) Equilibrium modulus of undoped-MWNT sponges is density independent at 30% compressive strain. (b) Equilibrium modulus of undoped-MWNT sponges increases with apparent density of sponge at 60% compressive strain. (c, d) Viscous modulus and relaxation time of undoped-MWNT sponges are density-independent (30% strain). Similar results were noticed at 60% strain (results not shown).**

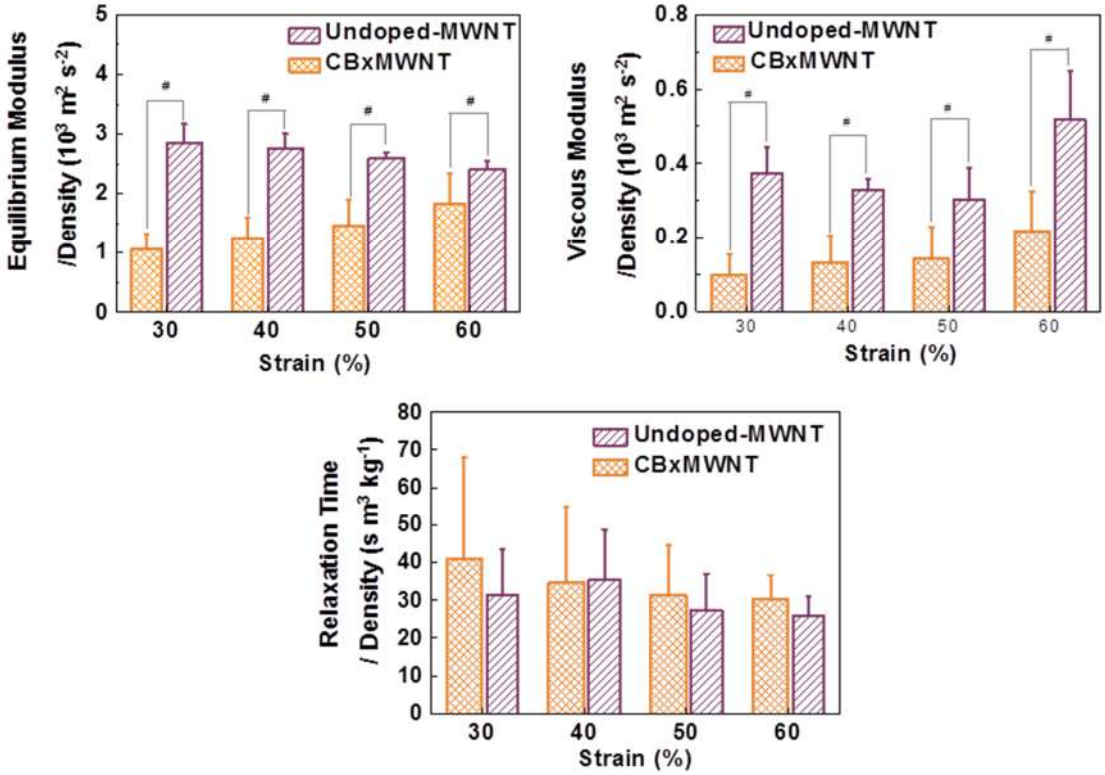

Figure 2.6 Comparison of density-normalized viscoelastic properties of CB_xMWNT and undoped-MWNT sponges at four different compressive strain levels. "#" denotes statistically significant differences ($P<0.05$). In order to compare the properties of two sponges without the effects of apparent density after fabrication, all viscoelastic properties were normalized by the density of the corresponding sample. Undoped-MWNT sponges have significantly higher equilibrium and viscous moduli than the CB_xMWNT sponges at all strain levels (30-60%). CB_xMWNT sponges exhibit strain-dependent equilibrium and viscous moduli (confirmed with linear regression), while those of undoped-MWNT sponges remain relatively constant. No statistical difference was detected between the relaxation time of the two types of sponge.

In addition to the static viscoelastic properties, dynamic viscoelastic properties of the two sponge types were characterized by DMA measurement. Similar to the static responses, DMA tests showed that the dynamic viscoelastic properties of the

CBxMWNT sponges are density-dependent (40% mean strain; 1% strain amplitude; 1Hz). The storage modulus, viscous modulus, and loss factor increase with increasing density (Figure 2.7a-b). In contrast, the behavior of the undoped-MWNT sponges is independent of density for all measured properties (Figure 2.8). This prominent disparity between the two sponge types has been confirmed under multiple mean strain levels (20%, 30%, and 50%). It is readily found that the storage modulus, as a measurement of the material's stiffness, increases with density. Meanwhile, CNT sponges with higher densities necessarily have increased inter-tube friction and energy dissipation due to air movement during cyclic compression, resulting in larger loss moduli. Moreover, the mechanism for a density-dependent loss factor may be related to the "zipping and unzipping" model reported previously, which interprets the dissipated energy as the energy consumed to overcome the large vdW attraction between CNTs in unzipping [19].

Another noticeable feature from Figure 4b is that the CBxMWNT sponges with a density of 28 mg/cm3 have a loss factor as high as 0.15 at 40% mean strain. Such a high loss factor is comparable to some cellular foams such as polyurethane foam [29], although the CNT sponge's density is much lower than those polymer materials. Indeed, the loss factors of the CBxMWNT sponges in the higher-density range exceed 0.1 for all the other mean strains (20%, 30% and 50%) (Figure 2.9). This observation is exciting, as it indicates the potential to fabricate a MWNT sponge with a high loss factor by controlling the density, which may have various applications, for instance, as a light biomaterial for the musculoskeletal system [30]. At a low mean strain, the loss factor of the undoped-MWNT sponges is comparable to that of the CBxMWNT sponges (Figure 2.7c). Above 30% mean strain, however, the

CBxMWNT sponge exhibits a significantly higher loss factor than the undoped-MWNT sponge. Therefore, in comparison with undoped-MWNT, the CBxMWNT sponges may function as a superior damping material under dynamic loading.

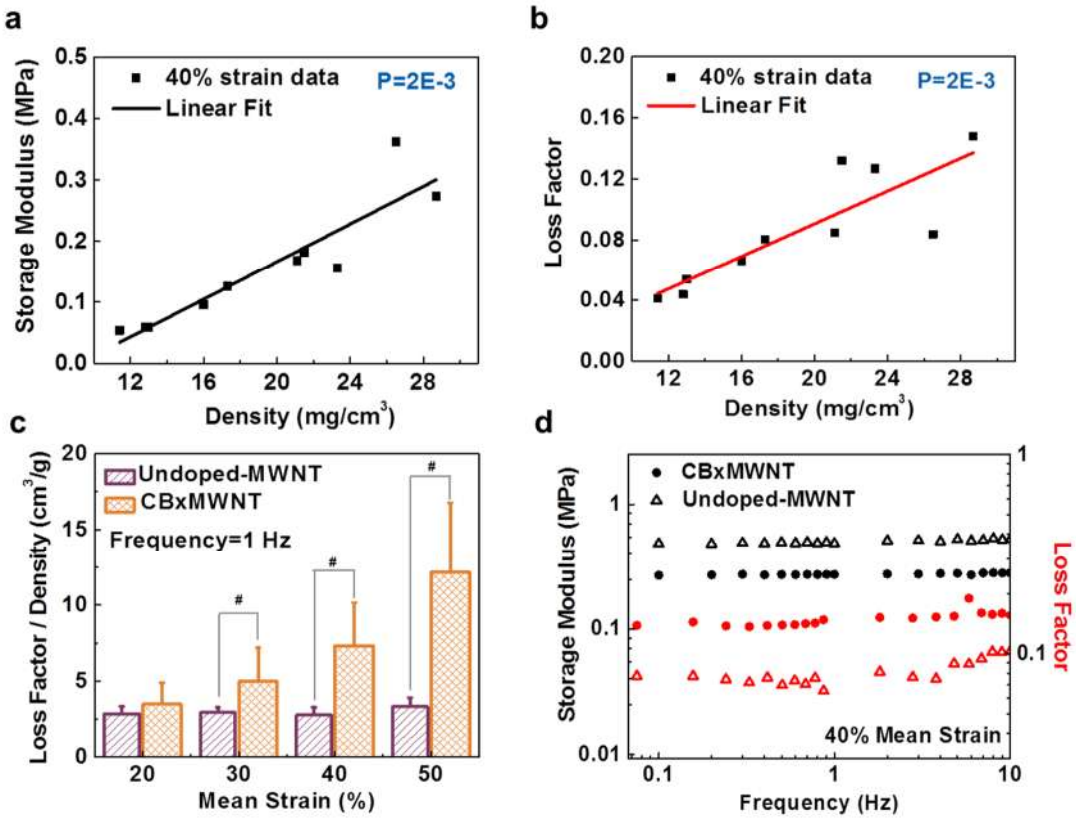

Figure 2.7 DMA characterization of CB_xMWNT and undoped-MWNT sponges. (a,b) Dynamic properties (storage modulus, loss modulus and loss factor) of CB_xMWNT sponges increase with density under dynamic loading at 1Hz and 40% mean strain with 1% strain amplitude. (c) Density-normalized loss factor of CB_xMWNT and undoped-MWNT sponges (# denotes statistically significance difference). (d) Representative dynamic properties (storage modulus, loss modulus, and loss factor) of both types of sponges plotted as a function of loading frequency (0.1 Hz-10 Hz) at room temperature. Density of CB_xMWNT and undoped-MWNT sponge sample is 26 and 29 mg/cm^3.

Figure 4d shows the invariant dynamic viscoelastic properties of both CNT sponges in the frequency range between 0.1 Hz to 10Hz (strain rate of 4E-3/s to 4E-1/s). A similar behavior was observed for CNT sponges undergoing DMA testing in a shear mode [19]. Such rate-independent behavior can be explained by unstable attachments/detachments process under the cyclic loadings. During each loading cycle, the CNTs are believed to have little time for energy dissipation [31]. Therefore, if CBxMWNT sponges with high loss factors are available as designed, the rate-independent viscoelastic behavior can broaden their application in engineering and biomedical fields [32–35].

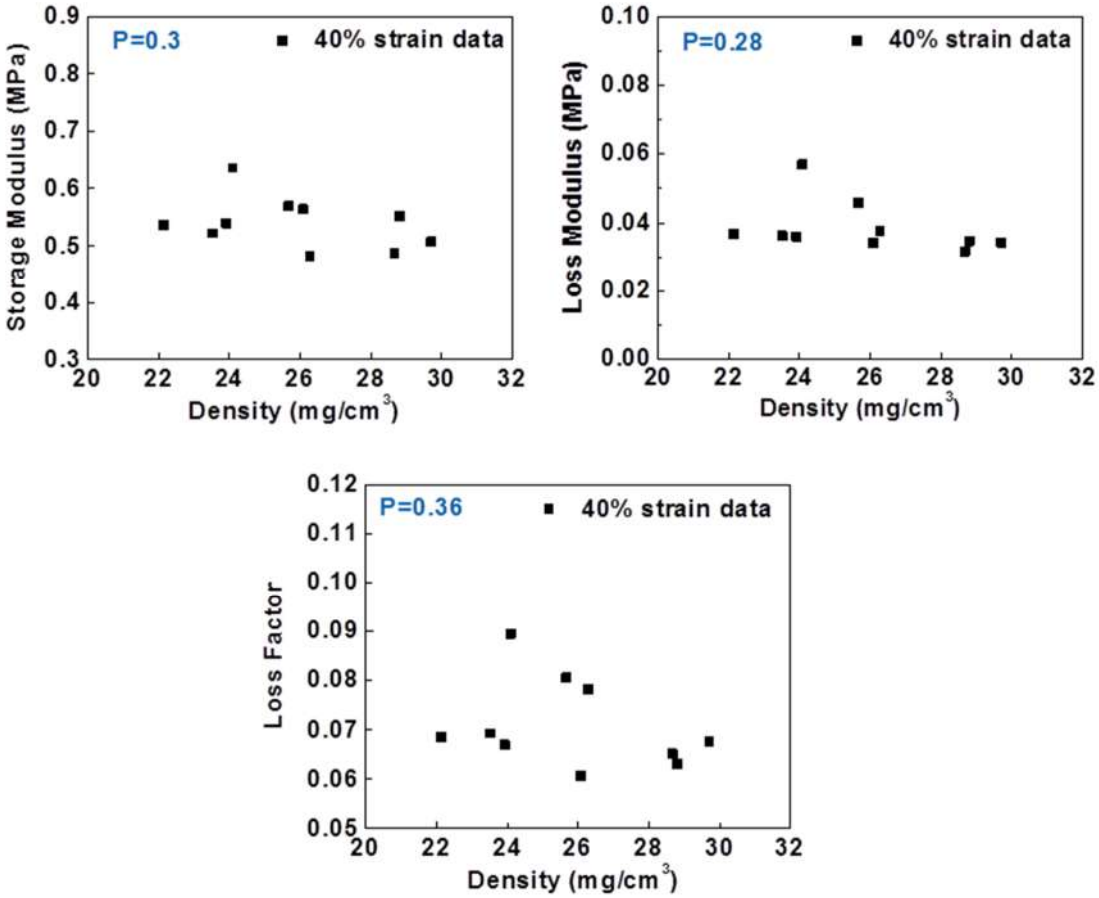

Figure 2.8 The dynamic properties of undoped-MWNT sponges measured by DMA, including storage modulus, loss modulus, and loss factor, are density-independent (40% mean strain; 1% strain amplitude; 1Hz). Similar results are found at mean strains of 20%, 30% and 50%.

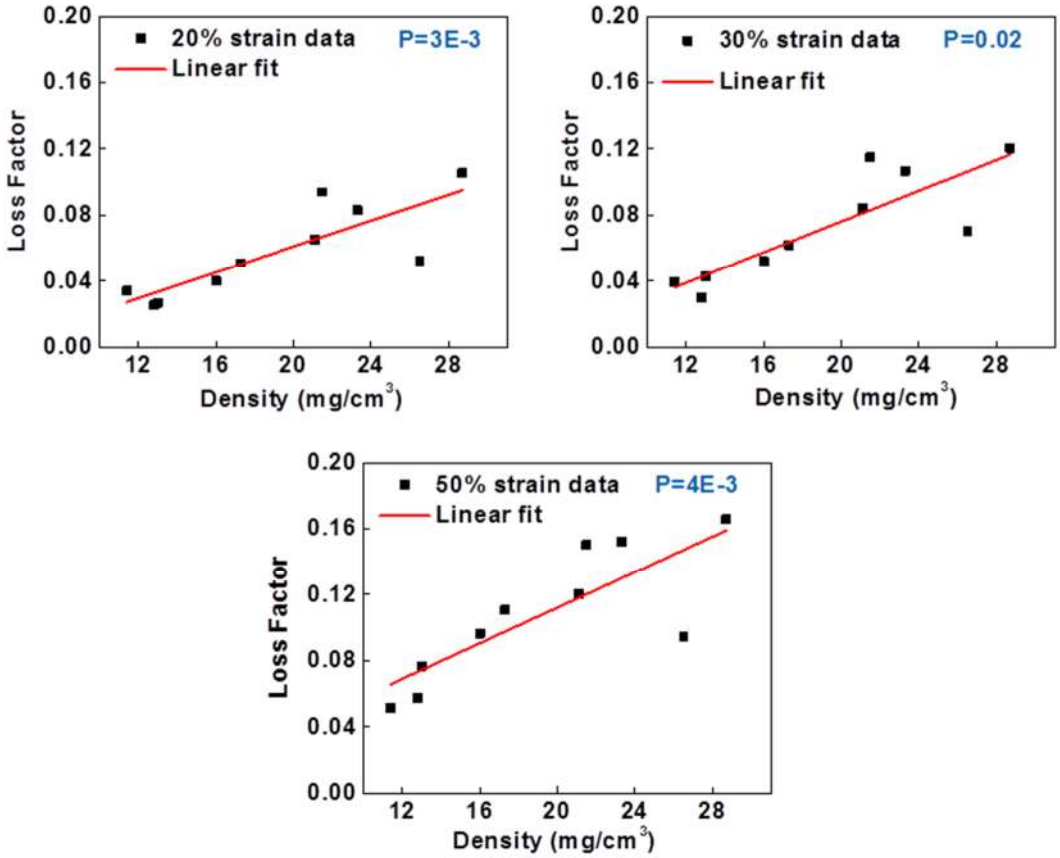

Figure 2.9 Loss factor of CB_xMWNT sponges increases with apparent density at three different mean strain levels (20%, 30%, and 50%) at 1Hz with 1% strain amplitude. P-values from linear regression are all smaller than 0.05. The loss factor of high density sponges goes well above 0.1, indicating good energy-absorbing capabilities.

In this chapter, mechanical behavior of 3D-networked undoped-MWNT and CBxMWNT sponges with atomic-scale junctions was characterized and compared. It was experimentally observed that CBxMWNT sponges exhibit less (and more stable) plastic deformation than undoped-MWNT sponges, which can be attributed to the outstanding resilience of CBxMWNT sponges endowed by their covalent junctions. The "elbow-like" junctions prevent the permanent buckling and bundling of CNTs

inside the 3D networks by “sticky” vdW interactions. Interestingly, the plastic deformation of CBxMWNT sponges is found to be density-independent while that of undoped-MWNT sponges varies with sponge density. In contrast, CBxMWNT sponges exhibit density-dependent properties in both their static and dynamic viscoelastic responses, an effect not seen in undoped-MWNT sponges. The viscoelastic parameters of both MWNT sponges are invariant with respect to environmental temperatures and loading frequency.

The measured mechanical properties reveal that the 3D CBxMWNT sponges with covalent junctions possess stable mechanical behavior, along with predictable and controllable viscoelastic properties. The exceptional properties of CNTs can be exploited in sponge architecture while controlling and optimizing their junctions. These three-dimensional CNT structures could be used in many critical applications, such as biomedical or precision devices, particularly those which require lightweight, and thermally-stable materials, with controllable viscoelastic properties.

REFERENCES

[1] D. Qian, G.J. Wagner, W.K. Liu, M.-F. Yu, R.S. Ruoff, Mechanics of carbon nanotubes, Appl. Mech. Rev. 55 (2002) 495–532.

[2] P.G. Collins, P. Avouris, Nanotubes for Electronics, Sci. Am. 283 (2000) 62–69.

[3] Y. Wu, N. Yi, L. Huang, T. Zhang, S. Fang, H. Chang, et al., Three-dimensionally bonded spongy graphene material with super compressive elasticity and near-zero Poisson's ratio, Nat Commun. 6 (2015).

[4] M. Crespo, M. González, A.L. Elías, L. Pulickal Rajukumar, J. Baselga, M. Terrones, et al., Ultra-light carbon nanotube sponge as an efficient electromagnetic shielding material in the GHz range, Phys. Status Solidi – Rapid Res. Lett. 8 (2014) 698–704.

[5] R.K. Das, B. Liu, J.R. Reynolds, A.G. Rinzler, Engineered Macroporosity in Single-Wall Carbon Nanotube Films, Nano Lett. 9 (2009) 677–683.

[6] S. Talapatra, S. Kar, S.K. Pal, R. Vajtai, L. Ci, P. Victor, et al., Direct growth of aligned carbon nanotubes on bulk metals., Nat. Nanotechnol. 1 (2006) 112–116.

[7] B.I. Yakobson, L.S. Couchman, Persistence length and nanomechanics of random bundles of nanotubes, J. Nanoparticle Res. 8 (2006) 105–110.

[8] X. Gui, J. Wei, K. Wang, A. Cao, H. Zhu, Y. Jia, et al., Carbon nanotube sponges., Adv. Mater. 22 (2010) 617–21.

[9] S. Nardecchia, D. Carriazo, M.L. Ferrer, M.C. Gutierrez, F. del Monte, Three dimensional macroporous architectures and aerogels built of carbon nanotubes and/or graphene: synthesis and applications, Chem. Soc. Rev. 42 (2013) 794–830.

[10] D.P. Hashim, N.T. Narayanan, J.M. Romo-Herrera, D. a. Cullen, M.G. Hahm, P. Lezzi, et al., Covalently bonded three-dimensional carbon nanotube solids via boron induced nanojunctions, Sci. Rep. 2 (2012).

[11] C. Shan, W. Zhao, X.L. Lu, D.J. O'Brien, Y. Li, Z. Cao, et al., Three-dimensional nitrogen-doped multiwall carbon nanotube sponges with tunable properties, Nano Lett. 13 (2013) 5514–5520.

[12] M.A. Worsley, S.O. Kucheyev, J.H. Satcher, A. V Hamza, T.F. Baumann, Mechanically robust and electrically conductive carbon nanotube foams, Appl. Phys. Lett. 94 (2009).

[13] X. Gui, A. Cao, J. Wei, H. Li, Y. Jia, Z. Li, et al., Soft, Highly Conductive Nanotube Sponges and Composites with Controlled Compressibility, ACS Nano. 4 (2010) 2320–2326.

[14] M.B. Bryning, D.E. Milkie, M.F. Islam, L. a Hough, J.M. Kikkawa, A.G. Yodh, Carbon Nanotube Aerogels, Adv. Mater. 19 (2007) 661–664.

[15] J.M. Romo-Herrera, M. Terrones, H. Terrones, S. Dag, V. Meunier, Covalent 2D and 3D Networks from 1D Nanostructures: Designing New Materials, Nano Lett. 7 (2006) 570–576.

[16] J. Li, C. Papadopoulos, J. Xu, Growing Y-junction carbon nanotubes, Nature. 402 (1999) 253–254.

[17] M. Terrones, F. Banhart, N. Grobert, J.-C. Charlier, H. Terrones, P.M. Ajayan, Molecular Junctions by Joining Single-Walled Carbon Nanotubes, Phys. Rev. Lett. 89 (2002) 75505.

[18] W.N. Findley, J.S. Lai, K. Onaran, R.M. Christensen, Creep and Relaxation of Nonlinear Viscoelastic Materials With an Introduction to Linear Viscoelasticity, North-Holland Publishing Company, 1977.

[19] M. Xu, D.N. Futaba, T. Yamada, M. Yumura, K. Hata, Carbon Nanotubes with Temperature-Invariant Viscoelasticity from –196° to 1000°C, Sci. . 330 (2010) 1364–1368.

[20] J.H. McDonald, Handbook of Biological Statistics, Sparky House Publishing, 2009.

[21] X. Gui, Z. Zeng, A. Cao, Z. Lin, H. Zeng, R. Xiang, et al., Elastic shape recovery of carbon nanotube sponges in liquid oil, J. Mater. Chem. 22 (2012) 18300–18305.

[22] M. Xu, D.N. Futaba, M. Yumura, K. Hata, Carbon Nanotubes with Temperature-Invariant Creep and Creep-Recovery from −190 to 970 °C, Adv. Mater. 23 (2011) 3686–3691.

[23] Q. Zhang, Y.C. Lu, F. Du, L. Dai, J. Baur, D.C. Foster, Viscoelastic creep of vertically aligned carbon nanotubes, J. Phys. D. Appl. Phys. 43 (2010).

[24] S.D. Mesarovic, C.M. McCarter, D.F. Bahr, H. Radhakrishnan, R.F. Richards, C.D. Richards, et al., Mechanical behavior of a carbon nanotube turf, Scr. Mater. 56 (2007) 157–160.

[25] J. Suhr, P. Victor, L. Ci, S. Sreekala, X. Zhang, O. Nalamasu, et al., Fatigue resistance of aligned carbon nanotube arrays under cyclic compression., Nat. Nanotechnol. 2 (2007) 417–421.

[26] F. Vizesi, C. Jones, N. Lotz, M. Gianoutsos, W.R. Walsh, Stress Relaxation and Creep: Viscoelastic Properties of Common Suture Materials Used for Flexor Tendon Repair, J. Hand Surg. Am. 33 (2008) 241–246.

[27] Y. Kameo, T. Adachi, M. Hojo, Transient response of fluid pressure in a poroelastic material under uniaxial cyclic loading, J. Mech. Phys. Solids. 56 (2008) 1794–1805.

[28] M. Xu, D.N. Futaba, M. Yumura, K. Hata, Tailoring Temperature Invariant Viscoelasticity of Carbon Nanotube Material, Nano Lett. 11 (2011) 3279–3284.

[29] S. Basu, Quasi-static and Dynamic Compression Behavior of Flexible Cellular Material, Cp.literature.agilent.com. (2012).

[30] X. Gui, Z. Lin, Z. Zeng, K. Wang, D. Wu, Z. Tang, Controllable synthesis of spongy carbon nanotube blocks with tunable macro- and microstructures., Nanotechnology. 24 (2013) 085705.

[31] X. Yang, P. He, H. Gao, Modeling frequency- and temperature-invariant dissipative behaviors of randomly entangled carbon nanotube networks under cyclic loading, Nano Res. 4 (2011) 1191–1198.

[32] J. Suhr, N. Koratkar, P. Keblinski, P. Ajayan, Viscoelasticity in carbon nanotube composites., Nat Mater. 4 (2005) 134–137.

[33] J. Qu, Z. Zhao, X. Wang, J. Qiu, Tailoring of three-dimensional carbon nanotube architectures by coupling capillarity-induced assembly with multiple CVD growth, J. Mater. Chem. 21 (2011) 5967–5971.

[34] M.D. Rao, Recent applications of viscoelastic damping for noise control in automobiles and commercial airplanes, J. Sound Vib. 262 (2003) 457–474.

[35] X. Wei, M.-S. Wang, Y. Bando, D. Golberg, Thermal stability of carbon nanotubes probed by anchored tungsten nanoparticles, Sci. Technol. Adv. Mater. 12 (2011) 044605.

Chapter 3

HYPERELASTICITY OF THREE-DIMENSIONAL CARBON NANOTUBE SPONGE CONTROLLED BY THE STIFFNESS OF COVALENT JUNCTIONS

3.1 Introduction

Carbon nanotubes (CNTs) possess extraordinary mechanical properties, structural stability, thermal conductivity, and electrical properties [1]. In order to promote the applications of the CNTs at macroscale, fabrication of high performance 3-D CNT-based architectures (i.e. sponges, forms and aerogels) attracts a lot of interests recently [2, 3]. Different from uniformly aligned CNT bundles or CNT films, 3-D sponges composed of randomly oriented CNTs have been fabricated to achieve isotropic material properties [4–6]. However, it remains a great challenge to fabricate CNT sponges that reflect the mechanical properties of individual CNTs. Previous studies have shown compressive modulus values of these sponges fall in the range of kPa [6]. In human body, through the control of topology and organization, collagen fibers can form into various tissues with drastically different mechanical functions, such as cartilage, ligament, and skin, by controlling their topology [7]. This fact encourages a natural hypothesis that optimizing the topology and ultrastructure of CNTs may generate unprecedented functional 3-D sponges for various applications.

An effective technique to tailor the CNT morphology and organization in forming 3-D sponges is to introduce non-hexagon structures into CNT graphitic layers through heteroatom doping, such as boron and/or nitrogen [8]. We have used this technique successfully in generating a 3-D boron-doped multi-walled CNT (CBxMWNT) sponge, in which the formation of atomic-scale ‘‘elbow-like’’ junctions in CNT reforms the nanotube into a 3-D multi-segment architecture [4]. Recently, we also synthesized 3-D nitrogen-doped CNT (N-MWNT) sponges by introducing

nitrogen into the CNT structures [6]. Although both 3-D CNT sponges demonstrate prominent hyperelastic properties with nonlinear stress-strain relationship, which makes them good candidates for load support with a shock absorption capability, they showed entirely different hyperelastic behaviors.

It is natural to speculate that the presence of junctions is a key factor in controlling the sponges' mechanical properties. For example, when musculoskeletal tissues in the human body fail under a traumatic overloading, such as ligament tear or meniscus rupture, they are mostly induced by the failure of interfibrillar junctions, not the collagen fibers themselves [9]. In particular, the collective behaviors of the CNT assemblies should be dependent on parameters such as the density of junctions along each nanotube, number of zigzag nanotubes in a unit volume, and the stiffness of the junctions [10]. However, actual roles of these parameters and their mechanical contributions remain largely elusive. The stress-strain curves of CNT sponges were mostly explained using linear elastic or viscoelastic models [5,11]. No proper constitutive model is available to correlate the mechanical behaviors of CNT sponges with the CNT morphology or junction properties. Due to the challenges involved in performing a bending test at the junction site, little information about the junction modulus is available. Thus, understanding the CNT sponge properties as functions of covalent junction-related characteristics would determine which junction-related parameters should be regulated, during the design and fabrication of 3-D CNT sponges, to achieve the desired mechanical properties.

In this chapter, the CBxMWNT and N-MWNT sponges were fabricated via boron and nitrogen doping during chemical vapor deposition processes, respectively. Mechanical behaviors of both 3-D CNT materials as well as their correlations with the

sponge densities and various CNT morphology parameters were systematically characterized. Inspired by the similarity between the hierarchical structures of CNT sponges and many natural biopolymer networks [12,13], we further proposed a hyperelastic constitutive model for 3-D CNT sponges in which each fiber can deform independently and move with the macroscopic deformation. The new constitutive laws are expressed in the form of a hyperelastic strain-energy function as an indication of the nonlinear stress-strain behaviors of each single nanotube and overall CNT sponges [14]. The model accurately describes the nonlinear stress-strain relationship observed in the mechanical testing of both CBxMWNT and N-MWNT sponges. It also captures the dependency between the hyperelasticity and apparent density of the materials. The correlation between the CNT diameter and compressive modulus of the N-MWNT sponges matches perfectly with the theoretical prediction and curve-fitting is not necessary. More importantly, for the first time, the effective modulus of junctions was predicted based on the morphology of CNTs and the bulk mechanical behaviors of sponges. Covalent junctions in CBxMWNT (~100 GPa) are much stronger than those in the N-MWNT (~20 GPa), which partially contributes to the higher compressive modulus of CBxMWNT sponge. This finding also matches the theoretical conjecture that the boron-carbon bond is stronger than the nitrogen-carbon bond, which remains technically challenging to measure. The constitutive model further reveals that increased concentration and enhanced stiffness of CNT junctions, and shorter CNT segments on each individual CNT chain can generate stronger hyperelastic 3-D CNT networks. Therefore, with fabrication, mechanical testing, and constitutive modeling, this study revealed the junction properties in 3-D CNT sponges and further quantified the effects of junction stiffness and junction-related morphological variations in the

hyperelasticity of materials. The results provide a fundamental knowledge base and benchmark to guide future design and fabrication of 3-D CNT architectures.

3.2 Methods

CBxMWNT sponges were grown onto the walls of a quartz tube furnace using ferrocene, toluene, and triethylborane under Ar gas at 860℃ via an aerosol-assisted catalytic CVD method [4]. N-MWCNT sponges were synthesized in a CVD system, where a mixture of ferrocene, thiophene and pyridine was injected into the furnace using a syringe pump [6]. The diameters of the N-MWCNTs were controlled by varying the concentration of thiophene. N-MWCNT sponges with CNT diameters of 40-110 nm, 60-140 nm, and 80-180 nm were synthesized in the presence of thiophene at concentrations of 0.25, 0.5, and 0.75 vol%, respectively. The morphology of CBxMWNT was characterized by the field emission scanning electron microscopy (FESEM) using a LEO1530 and an FEI Nova NanoSEM630, both operated at 5kV. The N-MWNT sponges were characterized by SEM mode of focus ion beam (Zeiss, Auriga 60). The sample analysis chamber was operated at a pressure of 10-9 Torr. The diameters of the CNTs inside the N-MWCNT samples were measured using SEM images.

Monotonic compressive testing was performed on CBxMWNT and N-MWNT sponges. Both types of samples were cut into 3 mm diameter cylinders using a Harris Micro-Punch (Ted Pella, INC.). The thicknesses of the samples were measured on a dynamic mechanical analyzer (DMA, Q800, TA Instruments) with a 0.01N preload and ranged from 0.8 to 2 mm. Weights of the samples were measured on a XP6 microbalance (Mettler-Toledo, INC), and the sample density was calculated as the ratio between measured weight and corresponding volume. CNT samples with

different densities were compressed quasi-statically (1μm/s) with up to 50% strain using a micro-testing apparatus. The compressions (0%, 10%, 20%, 30%, 40% and 50%) were also recorded by digital videos (Canon EOS Rebel T2i with extension tube) to capture the shape variation of sponges in both vertical (loading) and lateral directions. The radius of the sponge was measured at each loading strain to calculate the lateral stretch.

3.3 Results and Discussion

3.3.1 Constitutive Model

SEM characterization in Figure 3.1a shows that the 3-D CNT sponge consists of randomly orientated and entangled CNTs. The synergistic effect of the dopant atoms has induced drastic tubular changes along the tubes. The formation of ‘‘elbow-like’’ junctions transforms the nanotubes into a 3-D structure with multiple segments [6]. In terms of the microscopic structure and topology, each CNT is comparable to a polymer chain or collagen fiber in human tissues [7, 15]. Polymer chains are usually considered to be flexible, and the neighboring segments are joined by free hinges [16]. Since the persistence length and contour length of 3-D CNTs are comparable, the bending stiffness is not negligible when compared to the axial modulus [17]. Thus CNT should be categorized as semi-flexible filaments with similar mechanical characteristics to many biological macromolecules, such as the F-actin filament in cytoskeleton [12,18].

The worm-like chain (WLC) model, which describes a continuous elastic beam that curves with thermal fluctuation by considering the chain’s bending stiffness, is widely used for semi-flexible chains [16,19]. Previous studies also used the WLC

model for 2-D CNTs inside a CNT film [20]. However, the elbow-like junctions shown in Figure 1a act as hinges that clasp the adjacent CNT segments together. Therefore, the discrete persistent chain model, a discrete form of the WLC model, was adopted in this study to describe the mechanical behavior of a 3-D CNT. As illustrated in Figure 3.1b, the chain now consists of n discrete segments with each segment of length l. Elastic energy of the chain is contributed from the work done by the external force at the end of the chains and the bending energy of the bonds [15,21,22], which is a function of the elastic stiffness of joints and the deformation angle between segments [15]. In Figure 3.1b, θ_0, θ_1, R_0, and R represent the tilting angles between each segment and end-to-end distance of the chain at initial and deformed states, respectively. λ represents the stretch ratio, where $R_0 = \lambda \cdot R$. In this single CNT model, controllable parameters include the number of junctions, n, length of CNT segments, l, the stiffness of the CNT junctions, D, and the initial angles between neighboring segments, θ_0 (see Appendix for details).

A CNT sponge can be essentially treated as a 3-D network of randomly oriented chains (Figure 3.1a). In this study, the orientations of CNTs in the sponge are categorized into three orthogonal directions where topological features are idealized to be identical, so that the constitutive law for CNT networks can inherit the framework of the conventional three-chain model (Figure 3.1c) [23]. Strain energy density of the network is the product of the chain density multiplied by the energy of a single CNT, which itself is correlated with the principle stretch of the material and also coupled with the sponge density.

Since a 3-D CNT sponge is a highly porous material that has significant volume reduction under compression, the strain energy of the CNT network should

include two components: an isochoric distortion-related part and a volumetric dilatation-related part [24–26]. In this study, the modified discrete persistent chain model was integrated with the compressive network model to accommodate both dilatation and distortion strain energies for the CNT network. The proposed new model was verified by the restrictions on the strain energy density function summarized by Ogden (see Appendix for details) [27]. Based on the energy function, stress-stretch correlation of the CNT network can be easily created. This correlates chain density, N, number of junctions, n, length of CNT segments, l, the stiffness of the CNT junctions, D, the initial angles between neighboring segments, θ_0, and a phenomenological parameter, m.

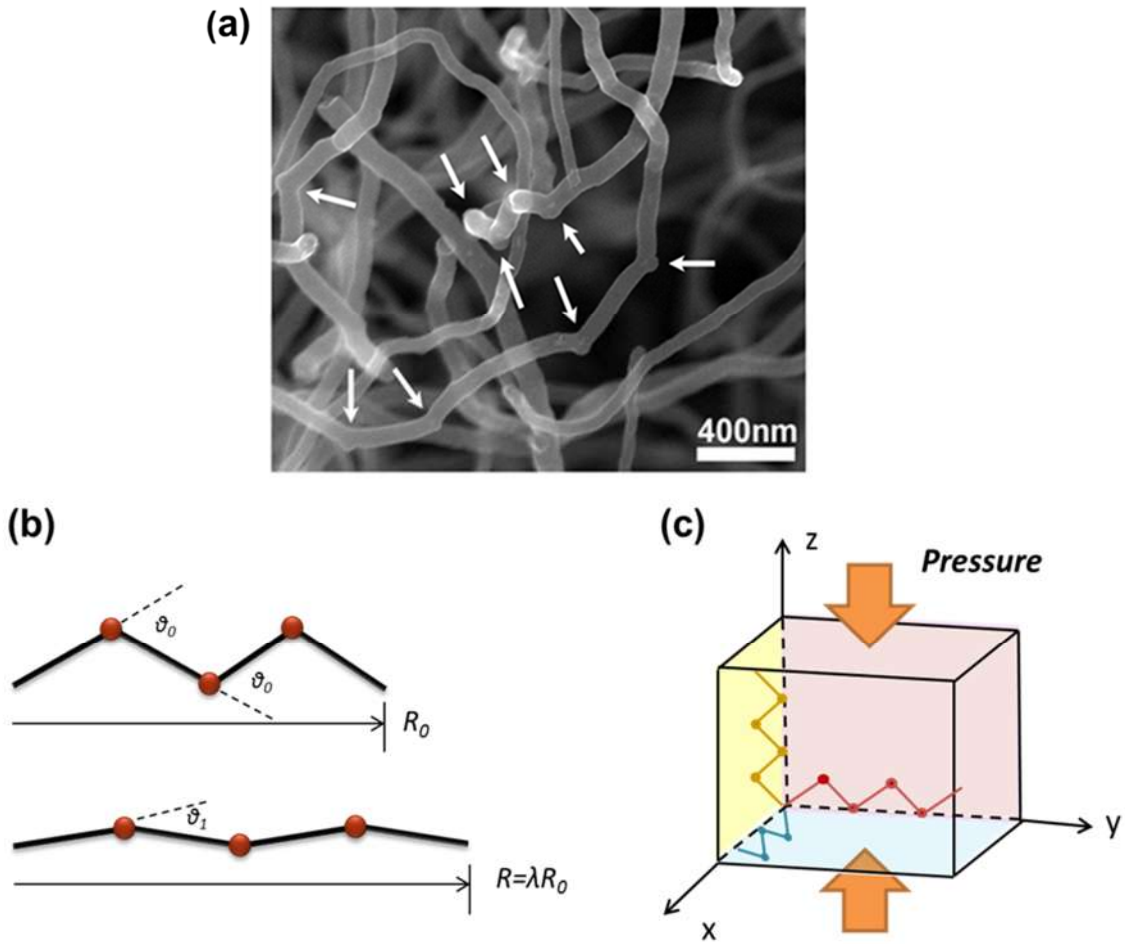

Figure 3.1 **(a) SEM image of CBxMWNT sponge. The observable "elbow" junctions are emphasized using white arrows. (b) Schematic of an idealized single CNT chain in initial and deformed states. Controllable parameters of the single chain model include number of junctions, n, length of CNT segments, l, the stiffness of the CNT junctions, D, and the initial angle between neighboring segments, θ_0. (c) An idealized CNT network with orthogonal aligned CNT chains. CNT chains are evenly projected into three orthogonal directions. Under a moderate compression, deformation of CNT sponge is assumed to be dominated by the CNTs parallel to the loading direction.**

3.3.2 Nonlinear Poisson's Effect of Sponges

According to the new constitutive model developed for 3-D CNT sponges in this study, a volumetric change or dilation of the material is dependent on the Poisson's behavior of a specific CNT material (Figure 3.2a). Figure 3.2b shows the photograph of the unconfined compression test on cylindrical sponge samples. Murphy's model was employed to capture the nonlinear Poisson's effect demonstrated in both types of sponges by describing the relationship between the axial stretch and lateral stretch (Figure 3.2c) [28]. According to the model, the correlation between axial and lateral stretches of some isotropic, nonlinear elastic materials may not simply follow the linear relationship with only one constant. Here, a nonlinear model with two coefficients was introduced to capture the lateral deformation as a function of the axial stretch in CNT sponges. The agreement between the experimental data and Murphy's model indicates that there is a unique nonlinear Poisson's ratio for both 3-D CNT sponges. Once the expression for lateral expansion of the material under loading is established, the corresponding volumetric change can be easily calculated and input in the constitutive model.

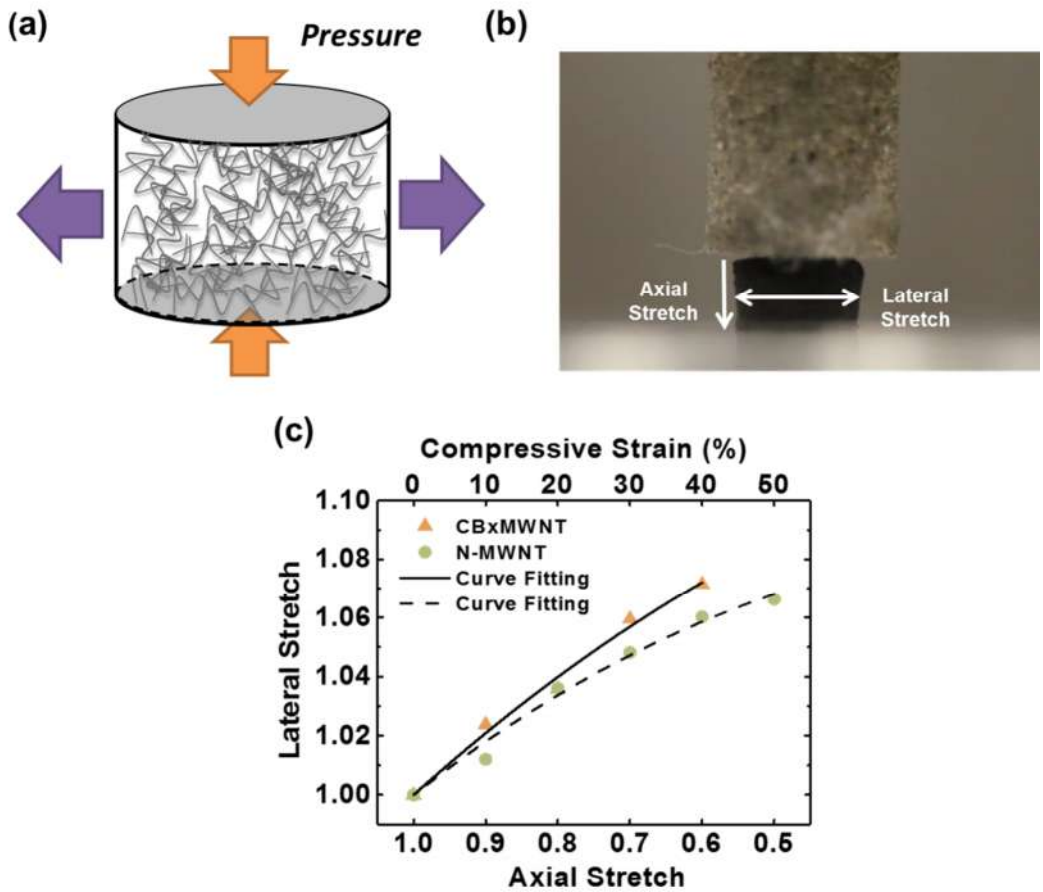

Figure 3.2 **(a) A schematic of 3-D CNT sponges under unconfined compression. The arrows indicate the principle compression and the lateral expansion of the sponge. (b) Photograph of a cylinder CBxMWNT sponge (3 mm in diameter and height varying from 0.8-2 mm) undergoing a uniaxial compression. (c) Experimental data of lateral stretch as a function of axial strain for CBxMWNT and N-MWTN sponges. Murphy's model provides excellent fit to the experimental data (solid and dash lines) [28].**

3.3.3 Properties of Covalently Bonded CNT Junctions

The modulus of the covalent junctions was determined by fitting the constitutive model to the stress-strain curves of 3-D CNT sponges under compression.

The average outer diameter for CNTs, d_o, is measured as ~70 nm and ~100 nm for CBxMWNT and N-MWNT, respectively. For both MWNTs, the inner diameter, d_i, is assumed as half of the corresponding outer diameter [4]. The contour and the segment length of CNT, L and l, were estimated at 10 μm and 500 nm, respectively, therefore the number of covalent junctions on a single chain is ≈ 20 ($n = L / l$). The chain density (number of CNTs per unit volume), N, was calculated as $\frac{\rho_{sponge}}{\rho_{CNT}} \cdot \frac{1}{V_{CNT}}$, where V_{CNT} is the volume of single CNT ($L \cdot \frac{\pi(d_o^2 - d_i^2)}{4}$). The density of individual CNT, ρ_{CNT}, was determined through its diameter and the number of layers.[29] The bending stiffness of the junction, D, is expressed as $D = EI$, where E and I represent the junction's effective modulus and moment of inertia, respectively. Experimental stress-strain curves for the CBxMWNT and N-MWNT sponges with different densities are shown in Figure 3.3. The data can be fitted perfectly with the new constitutive model ($R^2 > 0.99$). The effective moduli of the junctions in the CBxMWNT samples with densities of 34.5 mg / cm^3 and 24.5 mg / cm^3, was determined as 91.3 GPa and 118.3 GPa, respectively. The effective moduli of the N-MWNT junctions with densities of 34 mg / cm^3 and 40 mg / cm^3 were estimated at 22 GPa and 19.1 GPa, respectively. This indicates that the junction modulus in CBxMWNT was approximately 5 times greater than that of the N-MWNT, which matches the evidence that a boron-carbon bond is stronger than a nitrogen-carbon bond [30]. Since the doping of heteroatoms (boron or nitrogen) generates the elbow-like junctions that are considered to be defects along the CNT, it is not a surprise that the calculated effective moduli of both CBxMWNT and N-MWNT junctions are smaller than the Young's moduli of MWNTs [1]. This result also validates our initial hypothesis that a stretch along the

CNT axis rarely happens in a compressed sponge due to its incomparable stiffness compared to that of junctions. Moreover, the simulation output gives an insight into our previous observation that the 3-D CNT sponge with covalent junctions shows a comparatively smaller modulus than its pristine counterpart, undoped-MWNT sponges [11], while the presence of elbow-like junctions endows the sponge with controllable and remarkable mechanical flexibility. Considering that the junction stiffness could be regulated by the dopant materials, the creation of extraordinary 3-D CNT materials which possess both robust and flexible mechanical properties is promising.

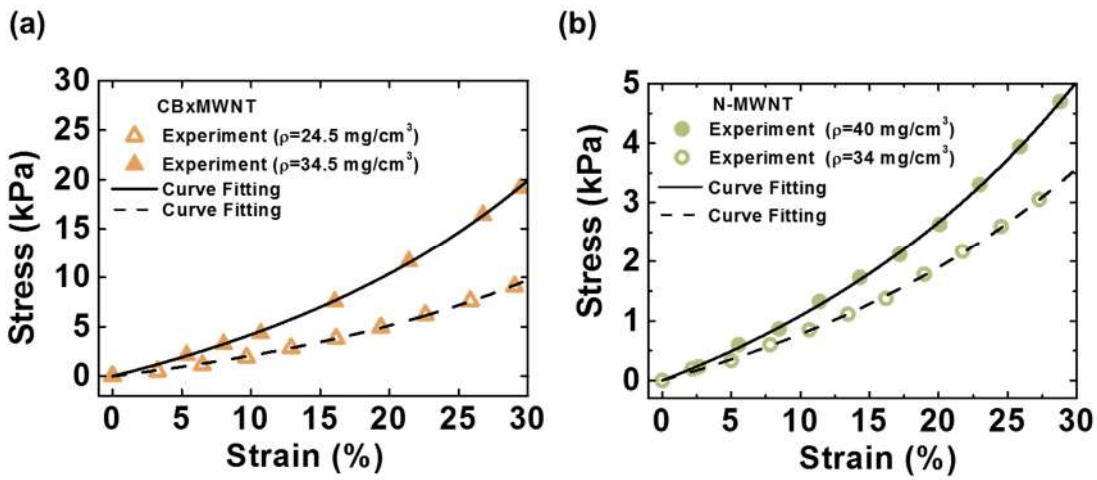

Figure 3.3 Experimental compressive stress-strain data of the (a) CBxMWNT and (b) N-MWNT sponges with different densities. The lines represent the curve fitting of the new constitutive model.

3.3.4 Density-Dependent Mechanical Behaviors

The experimental data demonstrated a density-dependent apparent modulus for the CBxMWNT sponge under compression, and a similar behavior was observed in the N-MWNT sponge. However, the influence of density to the apparent modulus

varies for different CNT sponges (Figure 3.4). To quantify this interplay relationship, we introduce two phenomenological parameters (m_0 and s) in the strain energy function, to relate the apparent density of the sponge to the bending of the CNTs inside (see Appendix for details). Again, the correlation between density and modulus can be accurately captured by the constitutive law (Figure 3.4b and c). By fitting the CBxMWNT and N-MWNT stress-strain curves, m_0 was determined as -0.08 and -0.042, and s was estimated at -71.3 and -94.4, respectively. Disparity in the parameters indicates different influences of a CNT's density on the apparent modulus of CNT networks. Here, the larger absolute value of s for N-MWNT implies that its apparent modulus is more sensitive to the density variation in comparison to the CBxMWNT sponge. Indeed the densities of as-fabricated N-MWNT sponges are much higher than those of CBxMWNT sponge samples (Figure 3.4b and c). Potential aggregation and excessive stretch of CNTs may result in a higher sensitivity of the apparent modulus for the density [5]. Therefore, by coupling the phenomenological parameters with the strain energy function, the proposed constitutive model is able to capture the density-modulus relationship for different CNT sponges.

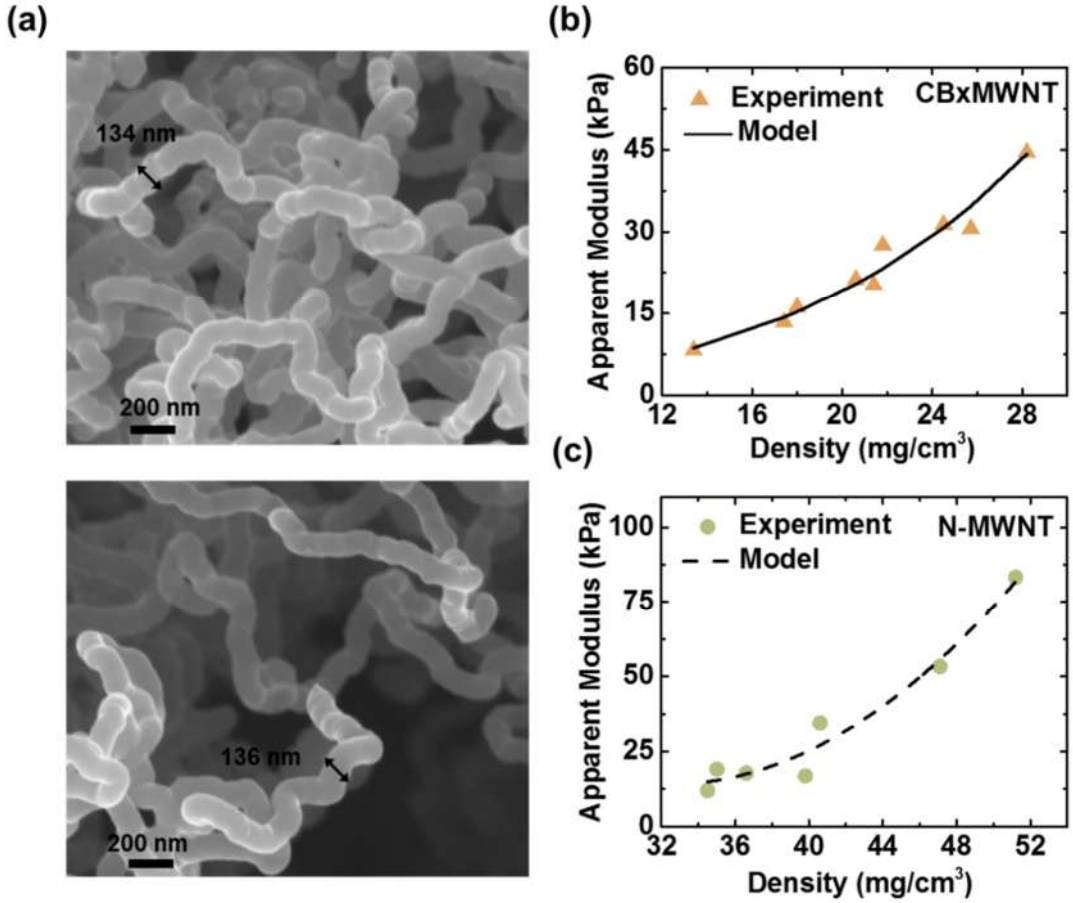

Figure 3.4 **(a) SEM images of N-MWNT sponges of controllable CNT diameter (≈ 135 nm) with different densities. (b, c) Experimental data and theoretical fitting of correlation between apparent modulus (measured at 30% strain) and density of CBxMWNT and N-MWNT sponges. For sufficient statistical power, nine CBxMWNT and seven N-MWNT samples were prepared and tested.**

3.3.5 Diameter of CNT

During the N-MWNT sponge fabrication, the average diameter of CNTs was successfully regulated by controlling the concentrations of thiophene [6]. When the density and other morphology parameters were kept constant, increasing the diameter of N-MWCNT could result in a larger apparent modulus of the sponge (Figure

3.5Figure 3.5). Our proposed model also predicts that the apparent modulus is dependent on the diameter squared and the elastic modulus of the CNT junction. It has been proved that the elastic modulus of CNTs has a strongly nonlinear, diameter-dependent characteristic [31, 32]. Here, by assuming the CNTs and CNT junctions share a similar correlation between diameter and elastic modulus (see Appendix for details) [32], the diameter-dependent apparent modulus of N-MWNT sponges is predicted and drawn in Figure 5b. It is seen that the predictions agree surprisingly well to the independent experimental data [6].

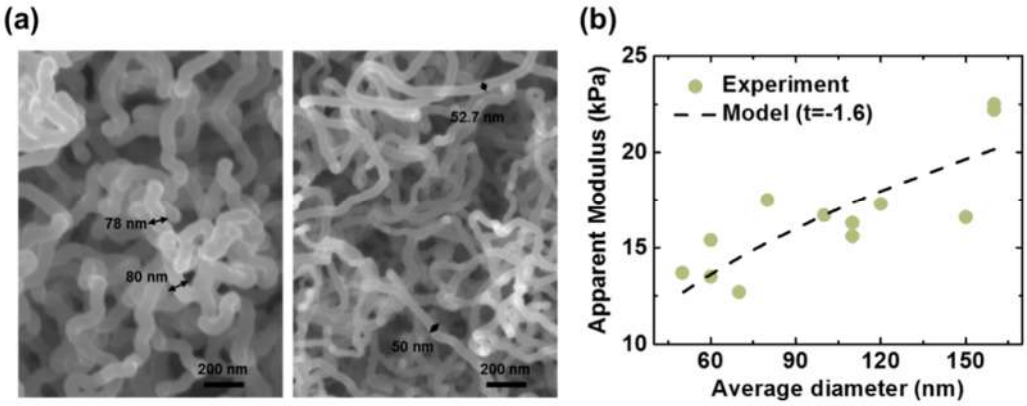

Figure 3.5 (a) SEM images of N-MWNT sponges with different average diameters (density ≈ 34.5 mg/cm3). The diameters of the CNTs were measured using SEM images. (b) Theoretical predication and independent experimental data of N-MWNT's apparent modulus as a function of CNT diameter. Note that the dash line is a pure predication instead of curve-fitting.

3.3.6 Number of Junctions and CNT Segment Length

Besides the experimentally reviewed correlations of 3-D CNTs, simulation with the constitutive model also predicts new structure-property relationships for 3-D

CNT networks. Results in Figure 3.6a and b demonstrate that the increasing number and modulus of the covalent junctions would generate a stronger 3-D CNT sponge. Importantly, when the contour length is kept constant, increasing the number of junctions has an quadratic effect on the apparent modulus, which is quantified as $E_B \propto n^2$.

The 3-D CNT sponges can also be strengthened with decreasing as-fabricated junction angle and CNT segment length (Figure 3.6c and d). It is worth noting that, for CNT networks with the same density, a shorter CNT segment length would result in a smaller CNT contour length and larger chain density. Thus, the apparent modulus of CNT network is related to the segment length as, $E_B \propto 1/l^2$, and can be remarkably enhanced with a shorter segment length if future synthesis techniques allow.

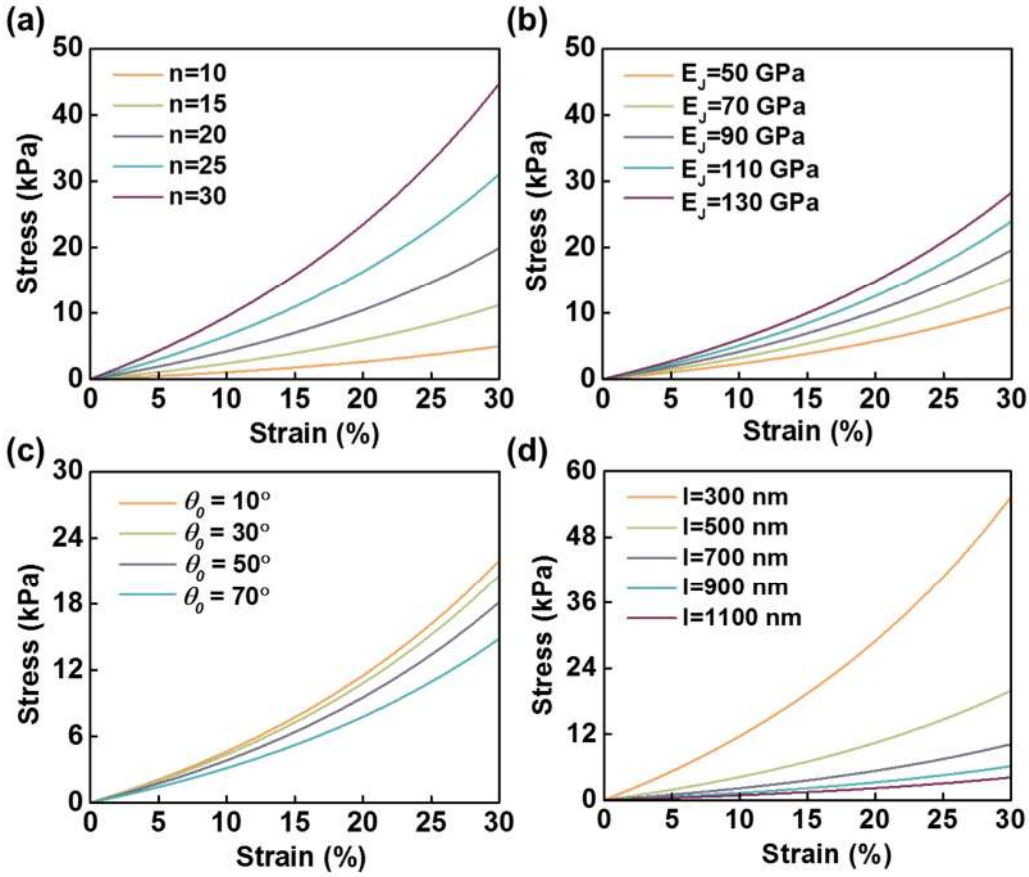

Figure 3.6 Effects of the (a) number of junctions and (b) elastic modulus of junctions on the stress-strain relationship of the CBxMWNT sponge (ρ_{sponge}= 34.5 mg/cm^3, d_0=70nm, L=10 µm, θ_0=37°). Effects of the (c) as-fabricated angle between neighboring CNT segments (d) CNT segment length on the apparent modulus of the CBxMWNT sponge (ρ_{sponge}= 34.5 mg/cm^3, d_0= 70 nm, n = 20, E_J= 91.3 GPa).

3.4 Conclusions

In summary, CBxMWNT and N-MWNT sponges' compressive behaviors were experimentally characterized as functions of morphology parameters, including

CNT diameter, density, and compressibility. A new microstructure-based constitutive law was established specifically for such isotropic 3-D CNT networks. The new model successfully adopts the contribution from the morphology parameters of CNTs as well as the stiffness of covalent-bonded junctions into the macroscale behaviors of the material. For the first time, the effective modulus of CNT junctions were obtained and compared between different doping atoms. The effective modulus of boron-doped covalent junctions is higher than that of the nitrogen-doped junctions. Moreover, the hyperelastic modulus of 3-D CNT sponges can also be controlled by the junction diameter, as well as the concentration of junctions or segment length of nanotubes. As the synthesis of controllable covalent bonding in 3-D CNT is still in its infancy, results from this work provide important guidance for the development of new fabrication techniques and the design of 3-D CNT materials.

3.5 Summary of Modeling of 3D CNT Sponge Network

3.5.1 Chain model of Single CNT

According to the discrete persistent chain model, the single CNT chain is regarded to consist of stiff segments which are connected by elastic joints. The CNT segment is assumed to be rigid due to its high tensile modulus when compared to the apparent modulus of networks [21,33]. Neglecting the force acting on rods, the sum of bending energy of all junctions gives the total energy of a single CNT chain, ε_0 [15].

$$\varepsilon_0 = \sum_{n=1}^{n-1} \frac{D}{l}(1-\cos\Theta_{i,i+1}) \tag{1}$$

where D represents the stiffness of the covalent junction and $\Theta_{i,i+1}$ is the angle between neighboring segments. For simplification, the single CNT is assumed to have uniform angles between neighboring segments (Figure 3.1b). According to Equation 1, the energy perturbation, $\Delta\varepsilon_0$, which is associated with the deformation of a CNT, can be expressed as

$$\begin{aligned}\Delta\varepsilon_0 &= \frac{D}{l}\cdot n\cdot\left|(1-\cos\theta_1)-(1-\cos\theta_0)\right| \\ &= \frac{D}{l}\cdot n\cdot\left|\cos\theta_0-\cos\theta_1\right|\end{aligned} \tag{2}$$

where θ_0 and θ_1 represent the tilting angles between each segment of the chain at initial and deformed states. The absolute symbol in the Equation 2 ensures the positive value of energy. By correlating the bending with the change of end-to-end distance of a CNT chain, Equation 2 can be reorganized as

$$\begin{aligned}\Delta\varepsilon_0 &= \frac{D}{l}\cdot n\,|\,\frac{2R_0^2}{n^2l^2}-\frac{2R_0^2\lambda^2}{n^2l^2}\,| \\ &= \frac{D}{l}\cdot n\cdot(1+cos\theta_0)\,|\,1-\lambda^2\,|\end{aligned} \tag{3}$$

The initial angle between CNT segments, θ_0, were estimated as 37° from SEM image (Figure 1a in main text). Therefore, the energy cost, associating with the bending deformation of CNT joints, is dependent on its bending stiffness, D, segment length, l, number of junctions, n , as-fabricated junction angle, θ_0 and the stretch ratio of CNT, λ .

The deformation ratios of an individual CNT and the 3D network in the k direction are represented as λ_k and δ_k , respectively. The relationship between λ_k and δ_k is defined as,

$$\lambda_k = \delta_k^{\ m} \tag{4}$$

where m is a phenomenological parameter. For a highly porous material as a CNT sponge [4], m should be proportional to the porosity of the 3D network,

$$m = m_0 \cdot (1 - \frac{\rho_{sponge}}{\rho_{CNT}})^s \tag{5}$$

where ρ_{CNT} and ρ_{sponge} are the densities of single CNT chain and the bulk sponge, respectively. Thus $1 - \frac{\rho_{CNT}}{\rho_{sponge}}$ is the porosity of the sponge network. The dimensionless parameters, m_0 and s, can both be determined by curve-fitting the experimental deformation data.

3.5.2 Constitutive Law for 3D CNT Sponge

The combination of Equations 3-5 yields the energy-strain function in the k direction,

$$\Delta\varepsilon_{0,k} = \frac{D}{l} \cdot n \cdot (1 + cos\theta_0) \cdot (\delta_k^{2m} - 1) \qquad k = x, y, z \tag{6}$$

The classical three-chain model regards the energy density of the network, $\Delta\varepsilon$, as a summation of work done in the three orthogonal directions, $\Delta\varepsilon = \Delta\varepsilon_x + \Delta\varepsilon_y + \Delta\varepsilon_z$ [23]. Therefore,

$$\Delta\varepsilon = \frac{N}{3} \cdot \sum \Delta\varepsilon_{0,k} = \frac{A}{3} \cdot (\delta_x^{2m} + \delta_y^{2m} + \delta_z^{2m} - 3) \tag{7}$$

where $A = N \cdot \frac{D}{l} \cdot n \cdot (1 + cos\theta_0)$, and N represents the chain density per unit volume of the CNT network. Different from incompressible polymer materials, the 3D CNT sponge is a typical porous elastic material, which undergoes significant volume change when compressed. Therefore both distortion energy, W_{incomp}, and dilatation

energy, W_{comp}, should be included in the strain-energy function [24-26]. An isotropic form of the strain-energy function for compressive materials at arbitrary strains can be written as [26],

$$W = W_{incomp} + W_{comp} = \sum \frac{c}{\alpha}[\lambda_1^{\alpha} + \lambda_2^{\alpha} + \lambda_3^{\alpha} - 3 + \frac{1}{\beta}(J^{-\alpha\beta} - 1)] \tag{8}$$

where $J = \delta_x \delta_y \delta_z$ and denotes the volume change under loading. The phenomenological parameters are α, β and c. For the CNT network, W_{incomp} is equal to $\Delta\varepsilon$. By comparing Equation 7 and Equation 8, the dilation energy function, W_{comp} can be represented as,

$$W_{comp} = \frac{2Am}{3} \cdot \frac{1}{p}(J^{-p} - 1) \tag{9}$$

where p is an phenomenological parameter analogous to β in Equation 8. Therefore, the final strain-energy density function for the 3D CNT network is

$$W = A \cdot [\frac{(\delta_x)^{2m} + (\delta_y)^{2m} + (\delta_z)^{2m}}{3} - 1 + \frac{2m}{3}(\frac{1}{p})(J^{-p} - 1)] \tag{10}$$

.

The proposed strain-energy function for the CNT network is further verified by the restrictions on the form of the strain-energy density function proposed by Ogden [24, 27], which include that 1) the strain energy density must be non-negative for all deformations; 2) the strain energy density must be minimum when there is no deformation ($\delta_k = 1$); and 3) the strain energy density must approach positive infinity at a singularity ($\delta_k = 0$).

Based on the strain energy function, the stress-strain relationship of a CNT sponge is,

$$f_k = \frac{J}{\delta_k}\sigma_k = \frac{J}{\delta_k}\frac{\partial W}{\partial \delta_k} \tag{11}$$

where f_k and σ_k represent the formal (nominal) stress and Cauchy (true) stress, respectively. Thus, the stress response of a CNT sponge under the load in the z direction, f_z, can be expressed as

$$f_z = \frac{J}{\delta_z} \cdot A \cdot (\frac{2m}{3} \cdot \delta_z^{(2m-1)} - \frac{2m}{3} J^{(-p-1)} \delta_x \delta_y) \tag{12}$$

Under unconfined compression, the lateral stretch of the CNT sponge is axially symmetrical (*i.e.*, $\delta_x = \delta_y$), while the lateral stress should be zero due the unconfined boundary condition ($f_x = f_y = 0$). The lateral stretch is then correlated to the principle stretch with

$$\frac{\delta_x^{2(m-1)}}{\delta_z} = J^{(-p-1)} \tag{13}$$

Therefore, the final stress-strain relationship for the CNT sponge becomes

$$f_z = \frac{J}{\delta_z} \cdot A \cdot \frac{2m}{3} \cdot (\frac{\delta_z^{2m} - \delta_x^{2m}}{\delta_z}) \tag{14}$$

The volume change or dilation of the material can be determined by the axial stretch, δ , and the corresponding lateral stretch, δ_L , using a power law relationship proposed by Murphy for isotropic elastic materials.

$$\delta_L = [-\nu(\delta^\gamma - 1) + 1]^{\frac{1}{\gamma}} \tag{15}$$

where, ν and γ are the material constants. Curve-fitting of the experimental data (Figure 3.2c) yields the parameters, ν=0.22 and γ=1.75 for the CBxMWNT sponge, and ν=0.19 and γ=2.1 for the N-MWNT sponge. The volume change of each material, J, can be written as a function of the axial stretch, δ, with the material parameters determined in Equation Figure 3.2.

3.5.3 Morphology and Modulus of 3D MWNT sponge

Experimental data disclosed that the apparent Young's modulus of a CNT sponge is dependent on the diameter of a single CNT [6]. Here, we adopt the expression of the area moment of inertia, $I = \frac{d_o^{\ 4}}{64}$, into the stress strain relationship (Equation 14). The apparent modulus, E_B, is then dependent on the outer diameter d_o as,

$$E_B \propto E_J(d_0) \cdot d_o^2. \tag{16}$$

$E_J(d_0)$ represents the elastic modulus of the CNT junction, which is strongly influenced by its varying diameter. Since the modulus of the 2D CNT decreases exponentially with the increasing diameter [31, 32], we propose that

$$\frac{E_1}{E_2} = (\frac{d_1}{d_2})^t \tag{17}$$

where d_1 and d_2 are different diameters of CNTs, and E_1 and E_2 are the corresponding moduli. According to a previous study [32], the value of t is estimated as -1.6. It is here assumed that the diameter's influence to the junction modulus is similar to that of the 2D CNT. Equation Figure 3.5 becomes

$$E_B \propto d_o^{2+t} \qquad (t = -1.6) \tag{18}$$

REFERENCES

[1] D. Qian, G.J. Wagner, W.K. Liu, M.-F. Yu, R.S. Ruoff, Mechanics of carbon nanotubes, Appl. Mech. Rev. 55 (2002) 495–532.

[2] J.M. Romo-Herrera, M. Terrones, H. Terrones, S. Dag, V. Meunier, Covalent 2D and 3D Networks from 1D Nanostructures: Designing New Materials, Nano Lett. 7 (2006) 570–576.

[3] S. Nardecchia, D. Carriazo, M.L. Ferrer, M.C. Gutierrez, F. del Monte, Three dimensional macroporous architectures and aerogels built of carbon nanotubes and/or graphene: synthesis and applications, Chem. Soc. Rev. 42 (2013) 794–830.

[4] D.P. Hashim, N.T. Narayanan, J.M. Romo-Herrera, D. a. Cullen, M.G. Hahm, P. Lezzi, et al., Covalently bonded three-dimensional carbon nanotube solids via boron induced nanojunctions, Sci. Rep. 2 (2012).

[5] X. Gui, A. Cao, J. Wei, H. Li, Y. Jia, Z. Li, et al., Soft, Highly Conductive Nanotube Sponges and Composites with Controlled Compressibility, ACS Nano. 4 (2010) 2320–2326.

[6] C. Shan, W. Zhao, X.L. Lu, D.J. O'Brien, Y. Li, Z. Cao, et al., Three-dimensional nitrogen-doped multiwall carbon nanotube sponges with tunable properties, Nano Lett. 13 (2013) 5514–5520.

[7] P. Fratzl, Collagen: Structure and Mechanics, Springer Science+Business Media, LLC, 2008.

[8] M. Terrones, F. Banhart, N. Grobert, J.-C. Charlier, H. Terrones, P.M. Ajayan, Molecular Junctions by Joining Single-Walled Carbon Nanotubes, Phys. Rev. Lett. 89 (2002) 75505.

[9] R.E. Brown, J.P. Butler, R.A. Rogers, D.E. Leith, Mechanical Connections Between Elastin and Collagen, Connect. Tissue Res. 30 (1994) 295–308.

[10] S. Dag, R.T. Senger, S. Ciraci, Theoretical study of crossed and parallel carbon nanotube junctions and three-dimensional grid structures, Phys. Rev. B - Condens. Matter Mater. Phys. 70 (2004) 205407.

[11] W. Zhao, A.L. Elias, L.P. Rajukumar, H.-I. Kim, D.J. O'Brien, B.K. Zimmerman, et al., Controllable and Predictable Viscoelastic Behaviors of 3D Boron-doped Multiwalled Carbon Nanotube Sponges, (n.d.).

[12] J.S. Palmer, M.C. Boyce, Constitutive modeling of the stress-strain behavior of F-actin filament networks, Acta Biomater. 4 (2008) 597–612.

[13] C. Storm, J.J. Pastore, F.C. MacKintosh, T.C. Lubensky, P.A. Janmey, Nonlinear elasticity in biological gels., Nature. 435 (2005) 191–194.

[14] S.P. Lake, M.F. Hadi, V.K. Lai, V.H. Barocas, Mechanics of a fiber network within a non-fibrillar matrix: Model and comparison with collagen-agarose co-gels, Ann. Biomed. Eng. 40 (2012) 2111–2121.

[15] J. Kierfeld, O. Niamploy, V. Sa-Yakanit, R. Lipowsky, Stretching of semiflexible polymers with elastic bonds, Eur. Phys. J. E. 14 (2004) 17–34.

[16] P.J. Flory, M. Volkenstein, Statistical mechanics of chain molecules, Biopolymers. 8 (1969) 699–700.

[17] H.S. Lee, C.H. Yun, H.M. Kim, C.J. Lee, Persistence length of multiwalled carbon nanotubes with static bending, J. Phys. Chem. C. 111 (2007) 18882–18887.

[18] R.C. Picu, Mechanics of random fiber networks—a review, Soft Matter. 7 (2011) 6768.

[19] J.F. Marko, E.D. Siggia, Stretching DNA, Macromolecules. 28 (1995) 8759–8770.

[20] Y. An, X. Li, B.Q. Wei, H. Jiang, A statistical mechanics model of carbon nanotube macro-films, Theor. Appl. Mech. Lett. 1 (2011) 041003.

[21] L. Livadaru, R.R. Netz, H.J. Kreuzer, Stretching response of discrete semiflexible polymers, Macromolecules. 36 (2003) 3732–3744.

[22] C. Storm, P.C. Nelson, Theory of high-force DNA stretching and overstretching, Phys. Rev. E. 67 (2003) 51906.

[23] L.R.. Treloar, The Physics of Rubber Elasticity, 3rd ed., Oxford University Press, 1975.

[24] M.M. Attard, Finite strain—isotropic hyperelasticity, Int. J. Solids Struct. 40 (2003) 4353–4378.

[25] J.E. Bischoff, E.M. Arruda, K. Grosh, A New Constitutive Model for the Compressibility of Elastomers at Finite Deformations, Rubber Chem. Technol. 74 (2001) 541–559.

[26] B. Storåkers, On material representation and constitutive branching in finite compressible elasticity, J. Mech. Phys. Solids. 34 (1986) 125–145.

[27] R.W. Ogden, Non-Linear Elastic Deformations, Dover Publications, 1997.

[28] J.G. Murphy, G.A. Rogerson, A method to model simple tension experiments using finite elasticity theory with an application to some polyurethane foams, Int. J. Eng. Sci. 40 (2002) 499–510.

[29] C. Laurent, E. Flahaut, A. Peigney, The weight and density of carbon nanotubes versus the number of walls and diameter, Carbon N. Y. 48 (2010) 2994–2996.

[30] R.T. Sanderson, Chemical bonds and bond energy, Academic Press, 1971.

[31] A.E. Tanur, J. Wang, A.L.M. Reddy, D.N. Lamont, Y.K. Yap, G.C. Walker, Diameter-dependent bending modulus of individual multiwall boron nitride nanotubes., J. Phys. Chem. B. 117 (2013) 4618–25.

[32] K. Lee, B. Lukić, A. Magrez, J.W. Seo, G.A.D. Briggs, A.J. Kulik, et al., Diameter-dependent elastic modulus supports the metastable-catalyst growth of carbon nanotubes., Nano Lett. 7 (2007) 1598–602.

[33] D. Qian, G.J. Wagner, W.K. Liu, M.-F. Yu, R.S. Ruoff, Mechanics of carbon nanotubes, Appl. Mech. Rev. 55 (2002) 495.

Chapter 4

VISCOELASTICITY IN THREE DIMENSIONAL CARBON NANOTUBES REINFORCED COMPOSITES

4.1 Introduction

In many applications including aerospace, automotive and biomedical science, there is an increasingly growing interest in the use of composite materials due to their high stiffness and strength-to-weight ratios [1,2]. The excellent properties of composites were interpreted as the result of load transfer from polymer matrix to fillers with much higher strength and stiffness [3]. The CNT, as a nanostructure with tensile modulus up to 1TPa [4], was also used to exploited as the filler phase in the composites [5–7]. It was found that the composites reinforced with vertical aligned CNT can generate more than an order of magnitude improvement in the modulus as well as damping capability [6]. However, ironically, a vertical aligned CNT composite's high stiffness and strength would offer undesirable unstable compressive response due to the local buckling behavior of CNTs. Meanwhile, the poor dispersion or unidirectional arrangement of CNT would give rise to the anisotropic properties which is not expected during application [8]. Therefore, 3D CNT materials seem to be an ideal filler for the composites because of the benefit from its isotropic and highly porous (e.g. >99%) characteristics [9–11].

Over the past decades, engineered three-dimensional (3D) CNT are one of the most compelling subjects under study. The 3D hierarchical CNT ultrastructure, in the macrostructure of porous sponge or aerogel, shows intriguing properties including unusual mechanical flexibility, ultralight weight, excellent electrical conductivity and super hydrophobicity [10–17]. The unique properties of the 3D CNT material seem to arise from the increase of active material per projected area, isotropic and homogenous

structure arrangement [12,16]. With the controlled ultra and macro-structures, the CNT based 3D assemblies can provides the applications ranging from environment-friendly reusable sorbent to aerospace structures as an energy absorption material [13,18].

The ultrastructure of the most as-fabricated 3D CNT materials are structured with randomly entangled CNTs [12,19–21]. Recently, covalently bonded 3D hierarchical CNT sponges have been successfully fabricated as well via chemical vapor deposition method [13,17]. It is predicted that by introducing the covalent junctions between CNTs, further CNT functionalization chemistry and superior mechanical properties can be achieved [13,22]. Our recent study shows that, the 3D CNT with covalent junctions exhibits controllable viscoelastic properties with excellent recovery ability when compared to its pristine counterpart. However, the functions of 3D CNT materials as the filler in the composite have not been unveiled. Hardly any data exists in literature that discusses role of covalent junctions in the 3D CNT when embedded in the polymer matrix.

With the curiosity of the application of 3D CNT composites, in this study, for the first time, we systematically investigated the elastic and viscoelastic properties of 3D CNT reinforcement polydimethylsiloxane (PDMS) composites via experimental characterization and modeling. Two types of CNT fillers were used in this study, which is 3D boron-doped multiwalled carbon nanotube sponges (CBxMWNT) and 3D multiwalled CNT without doping effect, referred as undoped-MWNT [12,13]. In addition, Mori–Tanaka method was employed in modeling the effective elastic properties of undoped-MWNT inside the composites.

4.2 Methods

4.2.1 Preparation of 3D CNT reinforced composite

Two types of 3D CNT sponges, CBxMWNT and undoped-MWNT, were synthesized according to previous studies [12, 13]. Both two types of sponges samples were cut into 3 mm diameter cylinders using a Harris Micro-Punch (Ted Pella, INC.). Then, the 3D CNT composite were fabricated following the methods in previous study [6]. The composites were prepared by infiltrating a polymer into the interstitial spaces of the cylinder-shaped CNT sponge via liquid-state polydimethylsiloxane (PDMS) premixture (DowSYLGARD 184 silicone elastomer and curing agent, weight ratio of 10:1). The infiltration process will be performed in a vacuum chamber at the pressure of 1 Torr for 12 hours. After the monomer infiltration, the composite would be left in an oven at 100 °C for postcuring.

The resultant composites consist of CNT sponge as reinforcement and the PDMS as the matrix. The composite samples were further cut into 2 mm diameter cylinders with 1~2mm in height. 10 samples of each material were prepared. A microbalance was used to measure the weight of each CNT and CNT composites samples. The weight volume fraction of the composites was calculated as the ratio between CNT samples and their corresponding composites.

4.2.2 Monotonic Compression Characterization

The cylindrical sample was mounted on a DMA (Q800, TA Instruments) fitted with 15 mm diameter platens at room temperature. An initial preload of 0.1 N was applied to the PDMS and composite samples in order to provide full contact between the loading platen and sample surface. The initial thickness of the sample was determined as the distance between the two platens under the applied preload. The

specimens were subjected to monotonic compression of different strain rate (1E-2/s, 1E-4/s) up to 40% strain.

4.2.3 Stress Relaxation Test and Viscoelastic Model

Stress relaxation tests were conducted with DMA Q800. The original length of the PDMS and composite sample was measured under the preload. During the stress relaxation test, a constant step displacement (product of original length and the targeted strain) was applied on the sample and held for 15 minutes (Figure 3a). The responsive force of the sample was recorded. The relaxation tests were performed at strain levels of 10%, 20%, 30%, and 40% strain.

The recorded stress-relaxation curves of each sample were fitted with a stretched exponential function model [23], $(t) = E_V \cdot e^{-\left(\frac{t}{\tau}\right)^k} + E_0 \quad (0 < k < 1)$, using MATLAB (MathWorks, Inc.). The distribution parameter k, was assumed to be 0.4 for all simulations at all strain levels [24]. The viscoelastic properties, including equilibrium compressive modulus E_0, viscous modulus E_V, and relaxation time τ, were determined from the curve fitting.

4.2.4 DMA Measurements

Frequency sweep tests were performed at 50°C, 35°C, 20°C, 5°C, -10°C, and -25°C in order to apply time-temperature superposition (TTS) to obtain data over a wider range of frequencies outside the capabilities of the DMA instrument (See Appendix for details). A frequency sweep over a range from 1 Hz to 30 Hz for each measurement. After measuring the initial length of the samples under the preload, samples were compressed to the mean strain of 5%. The samples were then cyclically compressed and released along their length at constant 1% strain amplitude, which

was within the linear region. To ensure the uniform distribution of temperature inside the sample, each sample was kept in the chamber 15 minutes before the measurement started. Four samples of each material were measured to provide a representative curve and reduce possible error from sample variation.

Temperature variation tests was performed on the samples on explore the viscoelastic behavior of each material over a wider range of temperature. The sample being tested was heated using the environmental chamber to a temperature of 75°C and held constant for 15 minutes to let the sample reach a uniform temperature. The sample was then compressed to the mean strain of 5%, and oscillated at the frequency of 1 Hz. The environmental chamber was then used to cool the sample at a rate of -5°C/min while being dynamically loaded.

4.3 Results

4.3.1 Compressive behavior Characterization and Modeling

The CBxMWNT and undoped-MWNT composites were prepared by infiltrating a polymer into the interstitial spaces of each CNT sponges via liquid-state PDMS premixture (see Methods). The morphology of both two CNT composites were first examined by SEM image (Figure 4.1a). It is observed that the intrinsic high porosity (the as-grown CNT sponges have only less than 1 vol% occupied by nanotubes, rest being empty/air) of the CNT sponges was completely replaced by the polymer matrix. The composite can be characterized as a randomly distributed CNT composite with about 0.7 vol% of CNTs. To investigate mechanical properties of the CNT composites, mechanical tests were performed with a Dynamic mechanical analysis (DMA) Q800 testing machine (see Methods). PDMS, CBxMWNT and

undoped-MWNT composite samples were cut into 1 mm radius and the thinkness ranged from 1 to 2 mm (Figure 4.1b). Compressive stress-strain behavior of the three different materials is shown in Figure 1c. Similar to early reports, the PDMS and CNT composites shows a nonlinear elastic behavior under compression [7]. The undoped-MWNT composites exhibits obvious increase in stiffness over the entire strain range. The undoped-MWNT composite has an apparent modulus of ~2.2 MPa between 0 and 6% strain, while pure PDMS and CBxMWNT show ~1.3 MPa. This is a remarkable 70% increase in modulus with only 1.5wt% undoped-MWNT as reinforcement. The enhancement can be explained as a synergetic effect between CNTs and the polymer matrix which taking the full use of high stiffness of CNTs [6]. Different from the undoped-MWNT composite, the CBxMWNT composite does not exhibit improved modulus at the toe region. The curvature in the CBxMWNT can eliminate the effective reinforcement when compared to straight CNT like undoped-MWNT [25]. Besides, the covalent junctions is similar to the crimp in the collagen fibrils [26], and it is not difficult to stretch out the crimp until the collagen fibrils become uncrimped. Thus as the strain increase, the CBxMWNT composite displays a sharp increase in stress response and shows comparable modulus as that of undoped-MWNT composite.

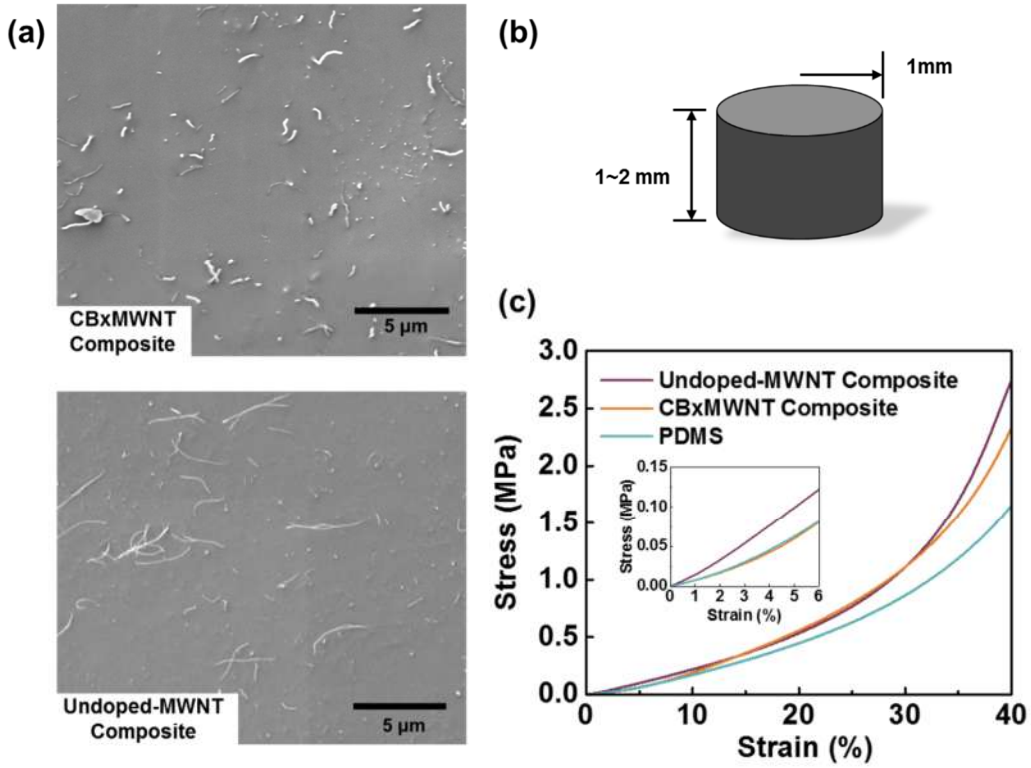

Figure 4.1 (a) SEM image of CBxMWNT and undoped-MWNT PDMS composite. (b) Schematic of cylinder PDMS and composite samples. (c) Monotonic compressive stress-strain curves of PDMS and two CNT composites with loading rate of 1E-4/s. The embedded plot magnifies the toe region of the stress-strain curve.

Motivated by characterization results showing that 1.5wt% undoped-MWTN yield an increase in the modulus of the composite on the order of 70%, here, we applied a traditional micromechanical method to determine the effective reinforcement modulus of a 3D undoped-MWNT. Mori-Tanaka (MT) model is one popular micromechanical method which approximates the behavior of multi-phase composites that contain reinforcements at non-dilute volume fractions [27]. The undoped-MWNT reinforced PDMS composite are considered as a two-phase composites containing randomly distributed cylinder inclusions with an infinite aspect ratio (See Appendix

for detail). The CNT and the PDMS matrix are modeled as linear elastic and isotropic, and perfect bonding between the interfaces is assumed. More detailed description of Mori-Tanaka model is discussed in previous study [28]. To determine the effective modulus of undoped-MWNT, the effective properties of CNT/PDMS for the use in the Mori-Tanaka method were measured or approximated. The Poisson ratio of the CNT and the PDMS was estimated at 0.16 [29] and 0.4995 [30]. As of the low volume fraction of CNT (0.7 %), the Poisson ratio of the composite was assumed to be same as that of PDMS. The apparent moduli (0~6% strain) of the PDMS and the undoped-MWNT were characterized as 1.3 and 2.2 MPa. The effective reinforce modulus of undoped-MWNT was then determined as 110 GPa, which was comparable to previous study of MWNT [31].

The investigation of the strain rate dependence was also performed on all the three materials. Figure 4.2a shows the representative stress-strain curve of PDMS under loading rate of 1E-4/s and 1E-2/s. The difference in elastic modulus from 1E-4/s to 1E-2/s strain rate is drawn in the Figure 2b. It can be seen that PDMS shows ~10% increase in modulus from lower to higher strain rate. However, such strain rate dependency of PDMS is reduced with the presence of CNT. Over the moderate strain level (e.g. 15%~30%), the CBxMWNT composite exhibits only ~5% increase in modulus. The undoped-MWNT composite, in a sharp contrast to the PDMS, shows negative difference which indicates that the higher loading rate could lead to even lower stress response of the undoped-MWNT composites. It can be concluded that, the molecular motions in PDMS which give rise to its rate-dependent characteristics of PDMS [32], are changed with the addition of CNTs. It should be noted that the influence of CNTs to the strain-rate dependence obviously varies for different 3D

CNT sponges. The lower stress of undoped-MWNT composite can be attributed to the potential fracture exists in the composite as a result of higher loading rate [33]. Therefore, the application of the PDMS polymer can be broadened by combining with the 3D CNTs when the invariant stress response under different loading rate is required.

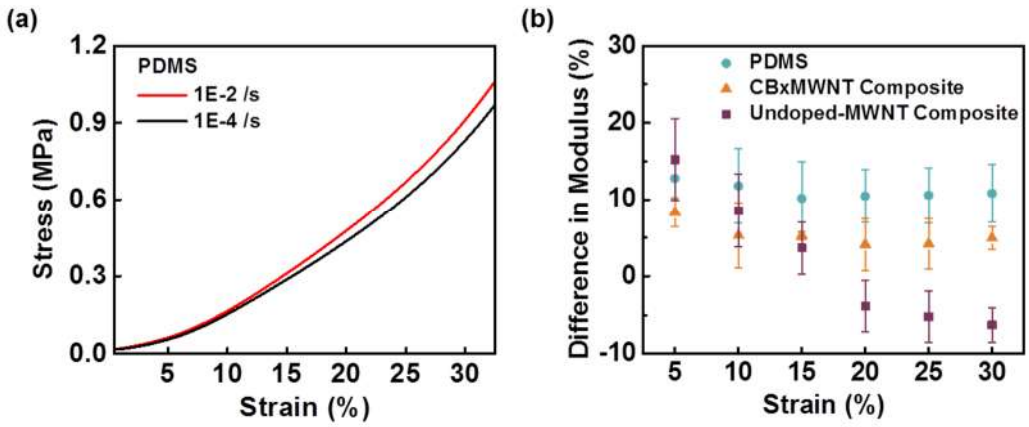

Figure 4.2 (a) Representative stress-strain behavior of PDMS under unconfined compression. (b) The difference in modulus, $(E_1 - E_0)/E_0$, for all three materials under different loading rate. E_1 and E_0 represent the modulus under loading rate of 1E-2/s and 1E-4/s, respectively.

4.3.2 Stress Relaxation Characterization

The stress relaxation responses, which are often referred to static viscoelastic properties, for both CNT composites and PDMS were quantified with equilibrium modulus, viscous modulus and relaxation time by employing stretched exponential function model (Figure 4.3a). Figure 4.3b-d summarize and compare the viscoelastic properties of both CNT composites and PDMS as a function of compressive strain

ranging from 10% to 40%. Student t-test were applied to identify the difference between the objects of comparison.

Figure 4.3b-c show that the CNT composites have significantly greater modulus in both equilibrium and viscous modulus over the PDMS baseline under the strains investigated in this study. It should be noted that, significant difference exist not only between PDMS and CNT composites, but also between CBxMWNT and undoped-MWNT composites. At 40% strain level, the improvement of viscous modulus from PDMS is quite substantial, at approximately 243%, for undoped-MWNT composites. As the tube-polymer sliding is considered to be the dominant mechanism for energy dissipation [34], undoped-MWNT with diameter of 16nm would introduce more interface and tube-polymer slippage between CNT and PDMS matrix than CBxMWNT which has average diameter of 69nm [11,13]. Besides, the undoped-MWNT composites shows an exponential increase in viscous modulus with respect to the strain while those of the undoped-MWNT sponges remain relatively constant according to our previous study [9]. Moreover, undoped-MWNT composite exhibit strain-dependent relaxation time, while that of CBxMWNT composite and PDMS remain relatively constant. The relaxation time τ is strongly dependent on the factors which effect the mobility of the material, and is roughly inverse to the rate of molecular motion. Previous study reported that by adding the unmodified CNT in the epoxy polymer, the mobility of the composite would increase and this may accounts for the decreasing relaxation time for undoped-MWNT composites under lager compressive strain [32]. The stress relaxation results indicate that by adding 3D CNT sponges in the PDMS polymer, the viscoelastic properties can be dramatically changed and are largely influenced by the morphologies of the different CNT fillers.

Importantly, the undoped-MWNT can endow the polymer remarkably enhanced equilibrium, viscous modulus and short relaxation time, which could be beneficial in many critical applications, such as biomedical or aircraft materials.

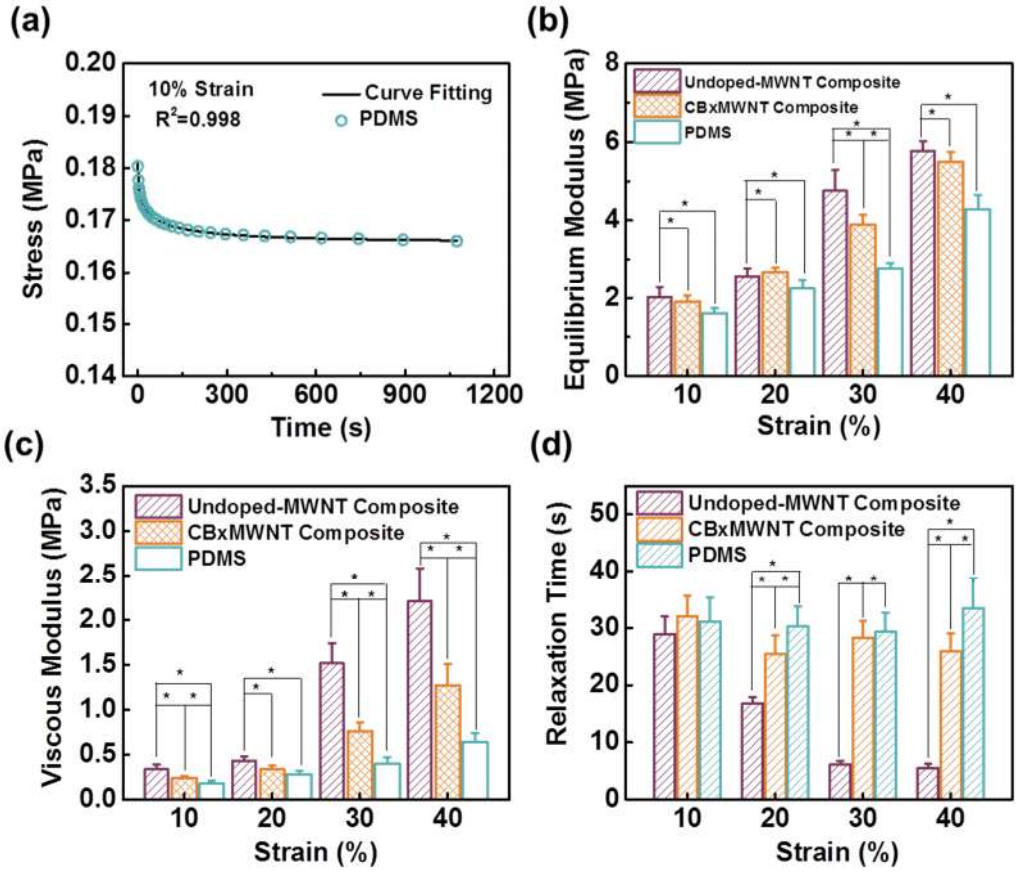

Figure 4.3 **(a) Representative curves of stress response of PDMS in stress relaxation test with curve fitting of stretch exponenti al model. The value R^2 attains 0.998 which quantifies an excellent curve fitting. (b-d) Elastic, viscous modulus and relaxation time of CBxMWNT, undoped-MWNT CNT composite and PDMS plotted as a function of strain. "*" indicates significant difference between objects of comparison as P value in student T-Test is less than the critical value ($P_{critical}$=0.05).**

4.3.3 Dynamic Viscoelasticity Characterization

In addition to the static viscoelastic properties, dynamic viscoelastic properties of the CNT composites and PDMS were characterized by DMA measurement. According to the principle of time temperature superposition (TTS), the viscoelastic response over a board range of frequency can be achieved by shifting the viscoelastic response at various constant temperatures along the log scale of frequency [35]. Therefore, frequency sweep tests was conducted from 1Hz to 30 Hz at temperatures from -25~50 ℃ (Figure 4a). Detailed information regarding the DMA measurement is provided in the methods section.

Figure 4.4a shows the storage modulus of PDMS as s function of the frequency measured at different temperature. By shifting the storage modulus-frequency curves at different temperature along the log scale of frequency, the master curve of the storage modulus was constructed as shown in Figure 4.4b (the base temperature was chosen as 20°C). Same measurements and TTS shifting were applied on CBxMWNT and undoped-MWNT PDMS composite samples. The storage modulus-frequency curves of both CNT composites and PDMS are shown in Figure 4.4c. All the three master curves exhibits frequency dependence and increase with respect to the frequency. It is readily found that the CNT composites have noticeable improvement over the PDMS, especially for undoped-MWNT composite. The enhancement in storage modulus between CNT composites and PDMS is comparable to the observation in equilibrium modulus. The results of temperature sweep test in Figure 4.4d indicates that the room temperature can be the best condition to take fully use of the large modulus of undoped-MWNT composite. The master curves of loss factor of

all the three materials are plotted as a function of log frequency in Figure 4.4e. The most remarkable feature from Figure 4e is that the undoped-MWNT composite displays significantly larger loss factor, which implies the damping abilities, than PDMS and CBxMWNT composite between 0.1 and 1000Hz. With the undoped-MWNT composite having loss factor values of 0.93 for frequencies of 0.1Hz, they are approximately 50% greater than those of either PDMS or CBxMWNT composite with 0.06 in loss factors. It should be noted that the loss factor of undoped-MWNT 0.25 at 1000 HZ, which is much higher than some sandwich composite being used as a noise-cancelling material [2]. Similar improvement of damping ability of undoped-MWNT composite was observed in the temperature sweep test as shown in Figure 4e. It can be seen that the undoped-MWNT composite keep a favorable high loss factor within a wide range of temperature from -75 to 75℃. Therefore, different from CBxMWNT composite, the undoped-MWNT composite can be seen as an ideal material with high damping ability with large modulus. Its potential application can endow improved fatigue properties and durability, allowing more service time under more severe loads until failure.

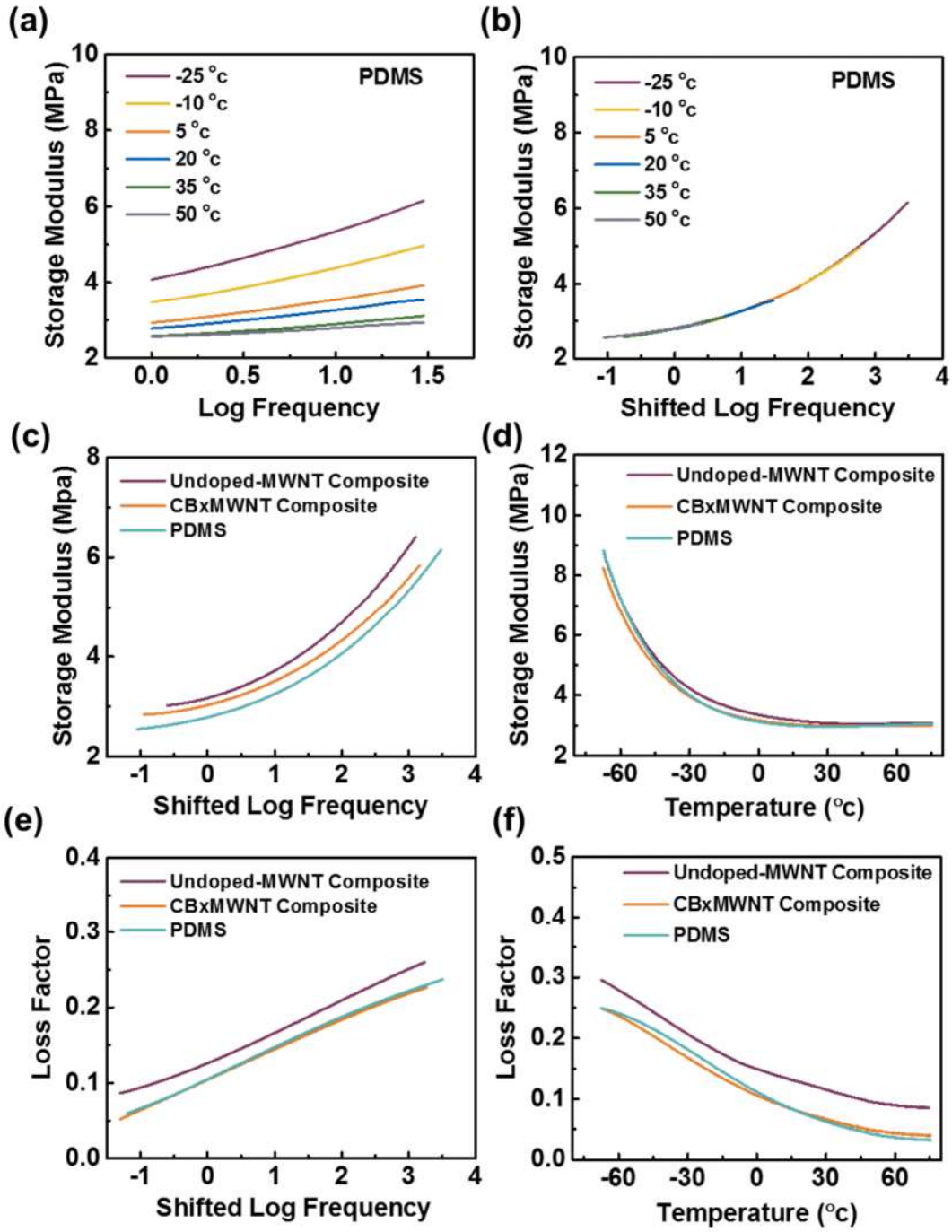
(a)
PDMS
-25 °c
-10 °c
5 °c
20 °c
35 °c
50 °c
Storage Modulus (MPa)
Log Frequency
(b)
PDMS
-25 °c
-10 °c
5 °c
20 °c
35 °c
50 °c
Storage Modulus (MPa)
Shifted Log Frequency
(c)
Undoped-MWNT Composite
CBxMWNT Composite
PDMS
Storage Modulus (Mpa)
Shifted Log Frequency
(d)
Undoped-MWNT Composite
CBxMWNT Composite
PDMS
Storage Modulus (MPa)
Temperature (°c)
(e)
Undoped-MWNT Composite
CBxMWNT Composite
PDMS
Loss Factor
Shifted Log Frequency
(f)
Undoped-MWNT Composite
CBxMWNT Composite
PDMS
Loss Factor
Temperature (°c)

Figure 4.4 (a) Representative curves of storage modulus of PDMS at different temperature. (b) Storage modulus master curve construction of PDMS. (c, e) Master curves of storage modulus and loss factor for PDMS, undoped-MWNT and CBxMWNT composite as a function of log frequency. (d, f) Storage modulus and loss factor with respect to temperature at 1HZ for PDMS, undoped-MWNT and CBxMWNT composite.

4.3.4 Conclusion

In this study, mechanical behavior of 3D CBxMWNT and undoped-MWNT reinforced PDMS composite, and pure PDMS was characterized and compared. It was experimentally observed that, with only ~1.5wt CNT in the PDMS matrix, the 3D undoped-MWNT composites can generate a remarkable improvement in the apparent modulus up to 70%. Furthermore, the undoped-MWNT composites exhibit 243% increase in viscous modulus over PDMS under 40% strain level. Interestingly, the undoped-MWNT composite exhibits a strain dependent relaxation time, which is much smaller than that of PDMS. Moreover, both TTS and temperature sweep tests show that the undoped-MWNT composites boast a remarkable improvement in damping performance, providing increased durability and lifetime operation. Therefore, marrying 3D CNT, especially undoped-MWNT with PDMS composite, provides a synergistic effect yielding a material with extraordinary viscoelastic feature and high damping capacity without sacrificing its mechanical performance. This may promote applications of 3D CNT sponges in biomedical material, in which biomimetic characteristic and reliable mechanical behavior are often desired for a long life.

4.4 Mechanical Characterization and Micromechanics Modeling

4.4.1 Time Temperature Superposition (TTS)

Time temperature superposition (TTS) is a conventional tool used for describing the viscoelastic behavior of linear polymers over a broad range of times or frequencies (in most case, beyond the measurement range of conventional instruments), by shifting data obtained at several temperatures to a preset reference temperature. The methods involves the use the temperature-dependent shift factors for the magnitudes for the time or frequency (horizontal shift factor) on log-log plots, such as relaxation, storage modulus and creep compliance [36]. Figure 4.5 shows construction of creep compliance master curve with raw data.

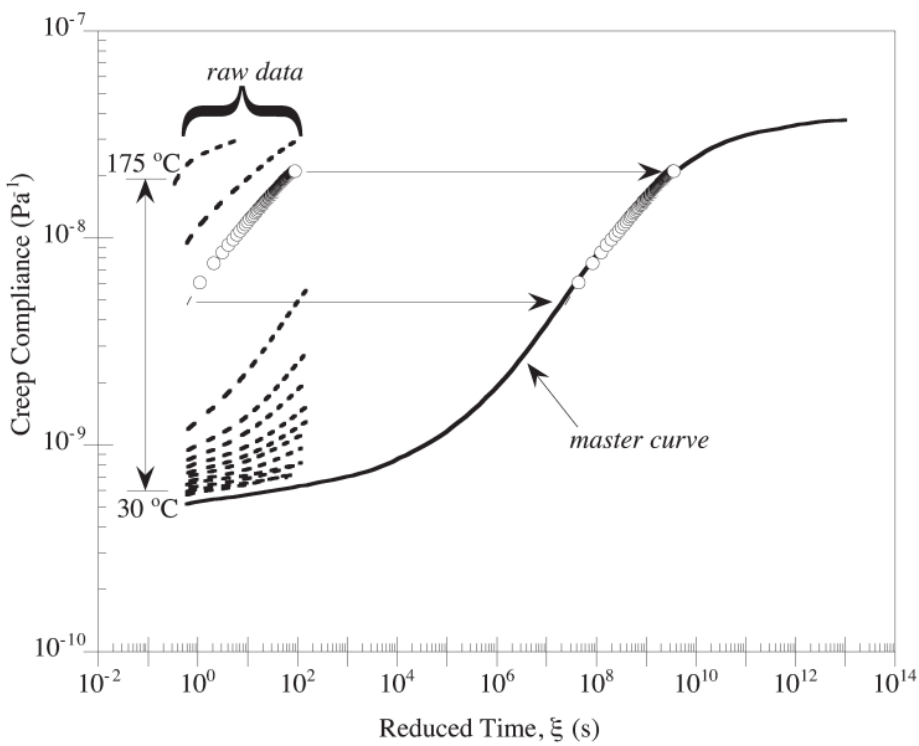

Figure 4.5 Creep compliance master curve construction, T_{ref}=30 ℃ [37].

Figure 4.5 show that data taken at different temperatures from 30 ℃ to 175 ℃ with reduced time of 3 decades. All the raw data curves are shifted horizontally to match up with data at a reference temperature (T_{ref}=30 ℃) and the consequent master curve covers 13 decades of time, which is out of reach of the experimental setup of DMA machine. The horizontal shifted distance is called the "shift factor", which is temperature-dependent. An empirical model, called Williams-Landel-Ferry (WLF) equation [35], was developed to estimate the shift factor for temperatures other than those for which the material was tested,

$$\log \alpha_t = \frac{-C_1(T - T_{ref})}{C_2 + (T - T_{ref})} \tag{4.1}$$

This equation uses the experimentally determined shift factors to solve for empirical parameter, C_1 and C_2. With C_1 and C_2, the shift factors can be determined for any reference temperature, and the viscoelastic curves can be shifted to a reference temperature of the any choice.

In this chapter, the TTS experiments was performed on 3D CNT composites and PDMS polymer, and the temperature dependent shift factor was determined as a function of temperature and fitted with WLF equation as shown in Figure 4.6. With the fitting curve in hand, the dynamic viscoelastic behavior in lager scales of frequency can be predicted without need of further experiments.

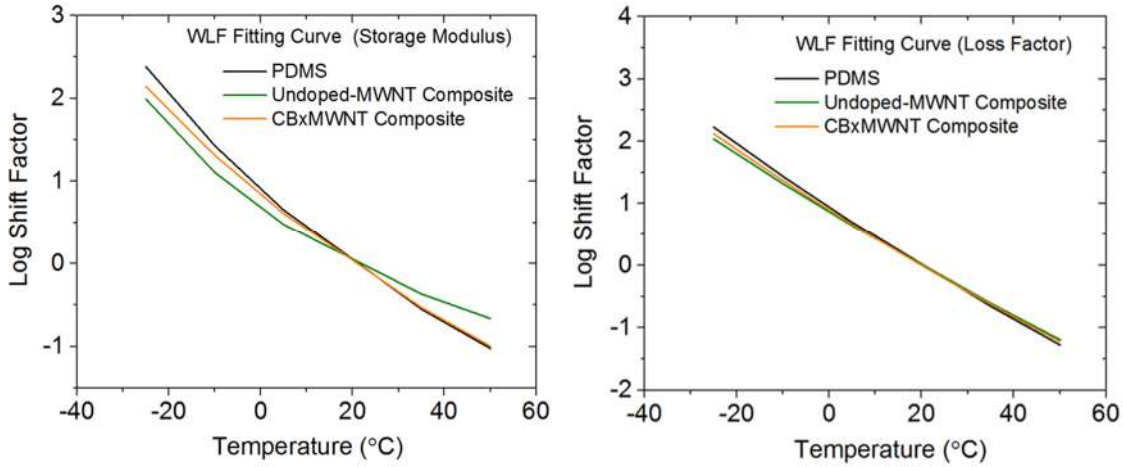

Figure 4.6 The curve fitting with WLF model for the shift factor of storage modulus and loss factor for CBxMWNT, undoped-MWNT composites and PDMS as a function of temperature.

4.4.2 Mori-Tanaka Method

The Mori–Tanaka method is an effective field approximation based on Eshelby's elasticity solution for inhomogeneity in infinite medium [38]. It has been used by a wide range of researchers to model the effective behavior of composites, and allows the average stress fields and overall effective stiffness of a composite with a non-dilute concentration of inclusions to be determined. The scheme of Mori-Tanaka model is shown in Figure 4.7.

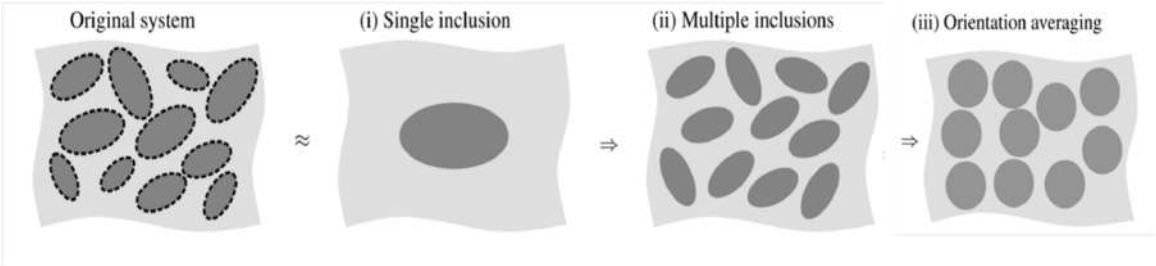

Figure 4.7 Mori-Tanaka based scheme: Strategy of derivation [39].

The effect stiffness tensor for the composite C is expressed as

$$C = C^m + v_f \left\langle (C^f - C^m) A^f \right\rangle (v_m I + v_f \left\langle A^f \right\rangle)^{-1} \tag{4.2}$$

Where v_f and v_m are the fiber and matrix volume fractions, respectively, **I** is the identity tensor, C^f and C^m are the stiffness tensor of the fiber and matrix, and A^f is the dilute mechanical strain concentration tensor for the fiber [28]. A^f accounts for inclusion interaction by relating the average matrix strain in the composite to the uniform applied strain,

$$\overline{\varepsilon_f} = A_f \overline{\varepsilon_0} \tag{4.3}$$

Where $\overline{\varepsilon_f}$ and $\overline{\varepsilon_0}$ are the average strain of fiber and matrix. The transformed dilute mechanical strain concentration tensor for the fiber with respect to the global coordinates is

$$\overline{A}^f_{ijkl} = c_{ip} c_{jq} c_{kr} c_{ls} A^f_{pqrs} \tag{4.4}$$

Where

$$\begin{aligned}
c_{11} &= \cos\phi \cos\psi - \sin\phi \cos\gamma \sin\psi \\
c_{12} &= \sin\phi \cos\psi + \cos\phi \cos\gamma \sin\psi \\
c_{13} &= \sin\psi \sin\gamma \\
c_{21} &= -\cos\phi \sin\psi - \sin\phi \cos\gamma \cos\psi \\
c_{22} &= -\sin\phi \sin\psi + \cos\phi \cos\gamma \cos\psi \\
c_{23} &= \sin\gamma \cos\psi \\
c_{31} &= \sin\phi \sin\gamma \\
c_{32} &= -\cos\phi \sin\gamma \\
c_{33} &= \cos\gamma
\end{aligned} \tag{4.5}$$

The orientation average of the dilute mechanical strain concentration tensor is [40],

$$\left\langle A^f \right\rangle = \frac{\int_{-\pi}^{\pi}\int_{0}^{\pi}\int_{0}^{\pi/2} \overline{A^f}(\phi,\gamma,\varphi)\sin(\gamma)\,\mathrm{d}\phi\,\mathrm{d}\gamma\,\mathrm{d}\varphi}{\int_{-\pi}^{\pi}\int_{0}^{\pi}\int_{0}^{\pi/2} \sin(\gamma)\,\mathrm{d}\phi\,\mathrm{d}\gamma\,\mathrm{d}\varphi} \tag{4.6}$$

The simplified the model, both PDMS matrix and MWCNTs are assumed to be isotropic. The parameters used in the Mori-Tanaka modeling are listed below,

	PDMS	**MWCNT**	**Undoped-MWNT Composite**
Young's Modulus (Mpa)	1.3	TBD	2.2
Possion Ratio	0.495	0.16	
Volume Fraction (%)			0.7
Aspect Ratio		500	

Table 4.1 Input properties of undoped-MWNT composites for Mori-Tanaka method

REFERENCES

[1] S.R. Bakshi, A. Agarwal, An analysis of the factors affecting strengthening in carbon nanotube reinforced aluminum composites, Carbon N. Y. 49 (2011) 533–544.

[2] J. Sargianis, H. Kim, J. Suhr, Natural Cork Agglomerate Employed as an Environmentally Friendly Solution for Quiet Sandwich Composites, Sci. Rep. 2 (2012).

[3] J. Nairn, On the use of shear-lag methods for analysis of stress transfer in unidirectional composites, Mech. Mater. 26 (1997) 63–80.

[4] S. Iijima, C. Brabec, A. Maiti, J. Bernholc, Structural flexibility of carbon nanotubes, J. Chem. Phys. 104 (1996) 2089–2092.

[5] E.T. Thostenson, Z. Ren, T.-W. Chou, Advances in the science and technology of carbon nanotubes and their composites: a review, Compos. Sci. Technol. 61 (2001) 1899–1912.

[6] L. Ci, J. Suhr, V. Pushparaj, X. Zhang, P.M. Ajayan, Continuous Carbon Nanotube Reinforced Composites, Nano Lett. 8 (2008) 2762–2766.

[7] J. Suhr, N. Koratkar, P. Keblinski, P. Ajayan, Viscoelasticity in carbon nanotube composites., Nat Mater. 4 (2005) 134–137.

[8] Y. Zeng, L. Ci, B.J. Carey, R. Vajtai, P.M. Ajayan, Design and reinforcement: Vertically aligned carbon nanotube-based sandwich composites, ACS Nano. 4 (2010) 6798–6804.

[9] W. Zhao, A.L. Elias, L.P. Rajukumar, H.-I. Kim, D.J. O'Brien, B.K. Zimmerman, et al., Controllable and Predictable Viscoelastic Behaviors of 3D Boron-doped Multiwalled Carbon Nanotube Sponges, (n.d.).

[10] J. Zou, J. Liu, A.S. Karakoti, A. Kumar, D. Joung, Q. Li, et al., Ultralight Multiwalled Carbon Nanotube Aerogel, ACS Nano. 4 (2010) 7293–7302.

[11] X. Gui, A. Cao, J. Wei, H. Li, Y. Jia, Z. Li, et al., Soft, highly conductive nanotube sponges and composites with controlled compressibility, ACS Nano. 4 (2010) 2320–2326.

[12] X. Gui, J. Wei, K. Wang, A. Cao, H. Zhu, Y. Jia, et al., Carbon nanotube sponges., Adv. Mater. 22 (2010) 617–21.

[13] D.P. Hashim, N.T. Narayanan, J.M. Romo-Herrera, D. a. Cullen, M.G. Hahm, P. Lezzi, et al., Covalently bonded three-dimensional carbon nanotube solids via boron induced nanojunctions, Sci. Rep. 2 (2012).

[14] S. Kabiri, D.N.H. Tran, T. Altalhi, D. Losic, Outstanding adsorption performance of graphene–carbon nanotube aerogels for continuous oil removal, Carbon N. Y. 80 (2014) 523–533.

[15] R.R. Kohlmeyer, M. Lor, J. Deng, H. Liu, J. Chen, Preparation of stable carbon nanotube aerogels with high electrical conductivity and porosity, Carbon N. Y. 49 (2011) 2352–2361.

[16] S. Nardecchia, D. Carriazo, M.L. Ferrer, M.C. Gutierrez, F. del Monte, Three dimensional macroporous architectures and aerogels built of carbon nanotubes and/or graphene: synthesis and applications, Chem. Soc. Rev. 42 (2013) 794–830.

[17] C. Shan, W. Zhao, X.L. Lu, D.J. O'Brien, Y. Li, Z. Cao, et al., Three-dimensional nitrogen-doped multiwall carbon nanotube sponges with tunable properties, Nano Lett. 13 (2013) 5514–5520.

[18] Z. Zeng, X. Gui, Z. Lin, L. Zhang, Y. Jia, A. Cao, et al., Carbon Nanotube Sponge-Array Tandem Composites with Extended Energy Absorption Range, Adv. Mater. (2012) n/a–n/a.

[19] M.A. Worsley, S.O. Kucheyev, J.H. Satcher, A. V Hamza, T.F. Baumann, Mechanically robust and electrically conductive carbon nanotube foams, Appl. Phys. Lett. 94 (2009).

[20] X. Gui, A. Cao, J. Wei, H. Li, Y. Jia, Z. Li, et al., Soft, Highly Conductive Nanotube Sponges and Composites with Controlled Compressibility, ACS Nano. 4 (2010) 2320–2326.

[21] M.B. Bryning, D.E. Milkie, M.F. Islam, L. a Hough, J.M. Kikkawa, A.G. Yodh, Carbon Nanotube Aerogels, Adv. Mater. 19 (2007) 661–664.

[22] J.M. Romo-Herrera, M. Terrones, H. Terrones, S. Dag, V. Meunier, Covalent 2D and 3D Networks from 1D Nanostructures: Designing New Materials, Nano Lett. 7 (2006) 570–576.

[23] G. Williams, D.C. Watts, Non-symmetrical dielectric relaxation behaviour arising from a simple empirical decay function, Trans. Faraday Soc. 66 (1970) 80.

[24] M. Zu, Q. Li, Y. Zhu, M. Dey, G. Wang, W. Lu, et al., The effective interfacial shear strength of carbon nanotube fibers in an epoxy matrix characterized by a microdroplet test, Carbon N. Y. 50 (2012) 1271–1279.

[25] F. Fisher, Fiber waviness in nanotube-reinforced polymer composites—I: Modulus predictions using effective nanotube properties, Compos. Sci. Technol. 63 (2003) 1689–1703.

[26] P. Fratzl, Collagen: Structure and Mechanics, Springer Science+Business Media, LLC, 2008.

[27] B. Mortazavi, M. Baniassadi, J. Bardon, S. Ahzi, Modeling of two-phase random composite materials by finite element, Mori-Tanaka and strong contrast methods, Compos. Part B Eng. 45 (2013) 1117–1125.

[28] F.T. Fisher, R.D. Bradshaw, L.C. Brinson, Fiber waviness in nanotube-reinforced polymer composites-I: Modulus predictions using effective nanotube properties, Compos. Sci. Technol. 63 (2003) 1689–1703.

[29] B.I. Yakobson, P. Avouris, Mechanical Properties of Carbon Nanotubes, Carbon Nanotub. 327 (2001) 287–327.

[30] I.D. Johnston, D.K. McCluskey, C.K.L. Tan, M.C. Tracey, Mechanical characterization of bulk Sylgard 184 for microfluidics and microengineering, J. Micromechanics Microengineering. 24 (2014) 035017.

[31] P. Poncharal, Z.L. Wang, D. Ugarte, W.A. de Heer, Electrostatic Deflections and Electromechanical Resonances of Carbon Nanotubes, Sci. . 283 (1999) 1513–1516.

[32] S.M. Yuen, C.C.M. Ma, C.C. Teng, H.H.O. Wu, H.C. Kuan, C.L. Chiang, Molecular motion, morphology, and thermal properties of multiwall carbon nanotube/polysilsesquioxane composite, J. Polym. Sci. Part B Polym. Phys. 46 (2008) 472–482.

[33] M.H. Moghim, S.M. Zebarjad, Effect of strain rate on tensile properties of polyurethane/(multiwalled carbon nanotube) nanocomposite, J. Vinyl Addit. Technol. (2014)

[34] L. Sun, R.F. Gibson, F. Gordaninejad, J. Suhr, Energy absorption capability of nanocomposites: A review, Compos. Sci. Technol. 69 (2009) 2392–2409.

[35] J.D. Ferry, S. a. Rice, Viscoelastic Properties of Polymers, Phys. Today. 15 (1962) 76.

[36] J. Dealy, D. Plazek, "Time-Temperature Superposition - A Users Guide," can be found under http://www.chem.mtu.edu/~fmorriso/cm4655/DealyPlazekTimeTempSuper2009.pdf.

[37] D. J. O'Brien, T. M. Patrick, S. R. White. "Viscoelastic properties of an epoxy resin during cure." Journal of composite materials 35.10 (2001) 883-904.

[38] J.D. Eshelby, The Determination of the Elastic Field of an Ellipsoidal Inclusion and Related Problems. Proceedings of the Royal Society A241 (1957) 376–396.

[39] Stránský J, Vorel J, Zeman J, Šejnoha M. Mori-tanaka based estimates of effective thermal conductivity of various engineering materials. Micromachines 2011;2:129–49.

[40] Fisher FT. Nanomechanics and the Viscoelastic Behavior of Carbon Nanotube-Reinforced Polymers. 2002.

Chapter 5

CONCLUSION AND FUTURE WORK

5.1 Summary of the Research Contributions

The exceptional mechanical and electronic properties predicted for the newly developed 3D CNTs material, combined with their highly porosity and low density, endow this new form of carbon an ideal material potential applications. Before these predicted extraordinary properties are fully realized, considerable basic research is necessary.

This dissertation covers the original work in the area of mechanical characterization and modeling of 3D CNTs. In chapter 2, the plastic and viscoelastic responses of 3D CBxMWNT sponges with covalent junctions were investigated and compared with that of undoped-MWNT sponges. The static and dynamic viscoelasticity of both materials were quantified and compared. It was concluded that the covalent junction endow CBxMWNT a totally different properties compared with the undoped-MWNT sponge. Therefore, in chapter 3, the roles of covalent junctions in CNTs in the hyperelastic properties of isotropic 3D CNT sponges were identified. Hyperelastic properties of two sponges, CBxMWNT, N-MWNT, were experimentally quantified as the functions of CNT morphology. A novel microstructure informed continuum constitutive law was developed specifically for such isotropic CNT sponges with junctions. Analyzing the experimental data with the new theory reveals the effective modulus of boron-doped and nitrogen-doped junction, and demonstrate that the junction stiffness and the junction-related morpholgy is a key factor in regulating the hyperelastic compressive modulus of the material. With the understanding of basic mechanical properties of 3D CNTs with different

ultrastructure, in chapter 4, 3D CNTs reinforced PDMS composites were fabricated and characterized. It was found that, by adding only 1.5 wt% CNTs into the PDMS polymer, both the elastic and viscoelastic properties have changed a lot. In addition, the effective elastic modulus of 3D CNTs without junctions was evaluation. Overall, from chapter 2-4, the elastic properties of three types of 3D CNTs sponge (CBxMWNT, N-MWNT and undoped-MWNT) with different ultrastructure, were characterized and estimated. For the first time, some structure/properties correlations for 3D CNT materials were characterized and established by modeling.

Some of the key conclusions and observation in this work are listed as follows:

In chapter 2, it is found that, under compression, the as-produced CBxMWNT sponges exhibit much less plastic deformation than undoped-MWNT sponges. Furthermore, the plastic deformation of CBxMWNT sponges is density-independent, while that of undoped-MWNT sponges increases with decreasing density. Thus the CBxMWNT sponges are more predictable and stable materials. Interestingly, CBxMWNT sponges display a density-dependent viscoelastic behavior under both static stress relaxation and dynamic cyclic loading tests, while the viscoelastic performance of undoped-MWNT sponges cannot be regulated by controlling sponge density. Dynamic mechanical analysis (DMA) testing showed that CBxMWNT sponges are thermally stable with loading rate-independent viscoelastic responses and high damping capabilities. Therefore, by optimizing the covalent junctions in 3D CNT sponges one could control and regulate their functional behavior. This may promote applications of 3D CNT sponges in biomedical or high-precision devices, in which lightweight and reliable mechanical behavior are often desired for a long life.

In chapter 3, hyperelastic properties of the 3D CNT sponges were experimentally quantified as the functions of CNT morphology. A novel microstructure informed continuum constitutive law was developed specifically for such isotropic CNT sponges with junctions. Analyzing the experimental data with the new theory demonstrated that, for the first time, the effective modulus of boron-doped junctions (~100 GPa) is higher than that of nitrogen-doped junctions (~20 GPa), and the junction stiffness is a key factor in regulating the hyperelastic compressive modulus of the material. Theoretical analysis further revealed that increased number of junctions and shorter segments on each individual CNT chains would result in stronger hyperelastic 3-D CNT networks. The study has established a fundamental knowledge base to provide guidance for the future design and fabrication of 3-D CNT macrostructures.

In chapter 4, it was found that by coupling 3D CNT with PDMS polymer, especially undoped-MWNT, would endow the polymer a remarkable improvement in elastic modulus (70%), viscous modulus (243%) and damping ability (50%). Besides, by applying Mori-Tanaka micromechanics model, the effective reinforcement modulus of 3D undoped-MWNT was estimated as 1.1 GPa, which is comparable to the conventional 2D CNTs. These results suggest that, if optimized, 3D CNT based composite could be an ideal material with reliable mechanical behavior which are often desired for a long service life.

5.2 Future work

This dissertation covered several novel aspects of 3D CNTs and their reinforced composites, including fabrication, characterization and modeling. As the controllable fabrication of 3D CNT with hierarchical topology is still in its fancy,

inspired suggestions for fabricating the 3D CNT with desired properties is necessary and urgent. Therefore, the full understanding of the mechanical characteristics of 3D CNTs and their polymer composites will enable us to further fabricate and utilize new hierarchical structures so as to establish novel solutions to limited application of CNTs in the industry.

In the research of CBxMWNT and undoped-MWNT sponges, we found that CBxMWNT exhibit much better resilience and predictable viscoelastic properties than that of undoped-MWNT sponge. However, with the similar density, the modulus of CBxMWNT is much lower than undoped-MWNT. It was found that in TEM that the quality of CBxMWNT in atomic scale is much lower than undoped-MWNT, including the area of junctions. The observation poses a challenge that to growth a "high-quality" 3D CNTs with less defects, which is comparable to their pristine counterpart. As the fabrication method as CVD processing is claimed to generate more defects in CNTs, suitable growth techniques with proper fabrication methods, and doping atoms have to be developed. The better experimental strategy could lead to their higher modulus, without sacrificing other properties. Meanwhile, advanced synthesis methods are desired to achieve 3D CNTs with controllable morphologies.

The continuous modeling evaluating the covalent junction stiffness was developed in this work. The model was able to describe the hyperelastic behavior of 3D CNT with junctions. However, it was found that for undoped-MWNT sponge, the stress-strain curve under compression is concave downward of which the slope decreases. The proposed model cannot represent the sharp contrast between the compressive behavior of undoped-MWNT and CBxMWNT sponges. The future work may focus on establishing a general modeling with physical meaning, which is able to

distinguish the 3D CNT with or without junction. The future model is expected to represent stress-strain behavior up to higher compression strain (i.e. 50%), of which the elastic or buckling behavior of the CNTs should be considered as well.

The literature review reveals that the elastic moduli of pristine CNTs were estimated direct measurements, of which the approach of AFM is the most straightforward. The introduction of heptagon-pentagon pair in the 3D CNTs creates the challenge of diriment measurement. Future work can focus on the characterization of 3D CNTs using AFM methods. In the study of 3D CNT PDMS composites, conventional Mori-Tanaka analytical model was used to evaluate the elastic properties of undoped-MWNT. For CBxMWNT composite, analytical or continuous model needs to be established to evaluate the effect modulus of CBxMWNT. Furthermore, By comparing the characterization with the modeling result, deep understanding of the elastic behavior of 3D CNTs can be achievement.

In the research of 3D CNT composite, different elastic and viscoelastic behavior was observed in composite with different 3D CNT fillers. Such interesting findings may attributed to the different interaction between CNT and the matrix. It is unknown whether the CNT junctions have a good/bad bond with the polymer matrix, and its influence to the mechanical behavior of the bulk composite. In addition, future work can focus on the load transfer between 3D CNTs and matrix as well. The mechanical behavior of the 3D composite under larger strain is unknown, and the potential debonding mechanism need to be detected and studied, which may indicate the corresponding debonding stress.

Overall, the research on the 3D CNTs is still in its initial stage, currently its potential application of is still limited to the environmental-friendly materials. In this

work , we found their controllable viscoelasticity and excellent damping properties which makes them ideal candidate for artificial biomaterial. Further study is crucial to help the development of 3D CNT and achieve more practical applications.